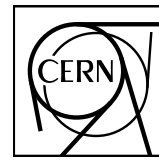


EUROPEAN ORGANIZATION FOR NUCLEAR RESEARCH



CERN-EP-2024-297

12 November 2024

System size and energy dependence of the mean transverse momentum fluctuations at the LHC

ALICE Collaboration*

Abstract

Event-by-event fluctuations of the event-wise mean transverse momentum, $\langle p_T \rangle$, of charged particles produced in proton–proton (pp) collisions at $\sqrt{s} = 5.02$ TeV, Xe–Xe collisions at $\sqrt{s_{NN}} = 5.44$ TeV, and Pb–Pb collisions at $\sqrt{s_{NN}} = 5.02$ TeV are studied using the ALICE detector based on the integral correlator $\langle\langle \Delta p_T \Delta p_T \rangle\rangle$. The correlator strength is found to decrease monotonically with increasing produced charged-particle multiplicity measured at midrapidity in all three systems. In Xe–Xe and Pb–Pb collisions, the multiplicity dependence of the correlator deviates significantly from a simple power-law scaling as well as from the predictions of the HIJING and AMPT models. The observed deviation from power-law scaling is expected from transverse radial flow in semicentral to central Xe–Xe and Pb–Pb collisions. In pp collisions, the correlation strength is also studied by classifying the events based on the transverse spherocity, S_0 , of the particle production at midrapidity, used as a proxy for the presence of a pronounced back-to-back jet topology. Low-spherocity (jetty) events feature a larger correlation strength than those with high spherocity (isotropic). The strength and multiplicity dependence of jetty and isotropic events are well reproduced by calculations with the PYTHIA 8 and EPOS LHC models.

© 2024 CERN for the benefit of the ALICE Collaboration.

Reproduction of this article or parts of it is allowed as specified in the CC-BY-4.0 license.

*See Appendix A for the list of collaboration members

1 Introduction

Studies of event-by-event fluctuations of event-wise observables measured in heavy-ion collisions are of great interest given that they probe the phase transition from quark–gluon plasma (QGP) to hadron gas (HG) [1–8]. Of particular interest are fluctuations of the average transverse momentum (p_T) of particles measured event-by-event in a specific kinematic range. These fluctuations are expected to be sensitive to energy fluctuations and, arguably, temperature variations of the matter produced in these collisions. In turn, the magnitude of these fluctuations is nominally proportional to the heat capacity of the hot medium, which is governed by the strong force as described by quantum chromodynamics (QCD) [9, 10]. As such, the temperature fluctuations are predicted to sharply increase in the vicinity of the critical point and near a cross-over phase transition boundary, as a result of a rapid change in the heat capacity of the medium near this boundary [9]. Fluctuations of the mean p_T , $\langle p_T \rangle$, are also highly sensitive to the presence of collective effects and the onset of thermalization in small systems. Measurements of $\langle p_T \rangle$ fluctuations are thus of great interest in the study of the hot and dense matter produced in heavy-ion collisions [3–5].

A significant number of measurements of $\langle p_T \rangle$ fluctuations have already been carried out at SPS [11–14] as well as at RHIC energies [15–21] based on a variety of observables. Traditionally, the measurement of $\langle p_T \rangle$ fluctuations is carried out in terms of the two-particle correlator, $\langle\langle \Delta p_T \Delta p_T \rangle\rangle$, which measures the particle momentum correlations based on deviations of p_T relative to $\langle p_T \rangle$ (discussed in Sec. 2). The ALICE Collaboration reported a measurement in Pb–Pb collisions at a center-of-mass energy per nucleon pair $\sqrt{s_{NN}} = 2.76$ TeV [22] using the $\langle\langle \Delta p_T \Delta p_T \rangle\rangle$ correlator. These prior measurements identified the presence of finite dynamical fluctuations corresponding to non-vanishing $\langle\langle \Delta p_T \Delta p_T \rangle\rangle$ correlations and additionally studied the evolution of the strength of the correlator with collision centrality. The interpretation of the observed fluctuations in terms of temperature fluctuations is, however, challenged by various considerations which are discussed below.

In small collision systems, one expects that the magnitude of the correlator $\langle\langle \Delta p_T \Delta p_T \rangle\rangle$ should be primarily determined by elementary particle production processes such as string fragmentation, hadronic resonance decays, and jets. The overall correlation strength measured in small collision systems should thus depend on the relative abundance of these processes and the relative strengths of the correlator for each of these processes. Correlations in large collision systems, on the other hand, should additionally depend on the number of individual nucleon–nucleon (or parton–parton) collisions and whether these produce collective phenomena or feature rescatterings of the particles they produce. For collisions involving independent nucleon–nucleon collisions, one expects that the strength of the correlator should evolve in inverse proportion to the number of sources of correlated particles, which is generally expected in a dilution scenario. The dilution results from the superposition of approximately independent particle-emitting sources, i.e., independent nucleon–nucleon collisions with no rescatterings of secondaries [23, 24]. This translates into an inverse dependence of the magnitude of the correlator on the average density of charged particles, $\langle dN_{ch}/d\eta \rangle$, produced in a given interval of collision centrality and pseudorapidity (η). Although prior observations of $\langle\langle \Delta p_T \Delta p_T \rangle\rangle$ at RHIC and LHC have shown that the magnitude of this correlator decreases monotonically from peripheral to central collisions, a sizable deviation from the $\langle dN_{ch}/d\eta \rangle$ scaling behavior was observed in semicentral to central collisions of large systems [17, 22, 25]. Fluctuations of the system energy (temperature) can evidently contribute to additional transverse momentum fluctuations and to a relative increase of $\langle\langle \Delta p_T \Delta p_T \rangle\rangle$, but a number of other mechanisms could potentially also explain the observed behavior. These include the onset of collectivity and thermalization [26, 27], string percolation [28], as well as initial-state energy density fluctuations [29–31]. Among these, the role of radial flow, well established from measurements of single-particle p_T distributions, may explain much of the deviation from inverse density scaling [26]. However, whether this deviation can be understood quantitatively on the basis of the aforementioned scenarios remains an open question. It is thus of interest to compare the collision centrality dependence of $\langle\langle \Delta p_T \Delta p_T \rangle\rangle$ observed in large collision systems with that found in elementary proton–proton (pp) col-

lisions. As stated above, in nucleus–nucleus (A–A) collisions, one expects that the scaling is primarily driven by the number of (binary) nucleon–nucleon (or possibly parton–parton) interactions resulting in an approximate linear scaling with the total produced multiplicity density. Such scaling is seemingly not expected in pp collisions, but one can nonetheless expect that the magnitude of $\langle\langle \Delta p_T \Delta p_T \rangle\rangle$ should evolve with the number of underlying correlated sources, whether these arise from string fragmentation, jet production, or multipartonic interactions. One must then examine in detail how the strength of $\langle\langle \Delta p_T \Delta p_T \rangle\rangle$ evolves with the particle density in both heavy-ion and pp collisions. Additionally, since stronger correlations are expected from the collimated particle production arising from the hadronization of jets, it is also of interest to compare the strength of the correlator in pp collisions by separating events with a pronounced back-to-back jet topology from events featuring approximately transversely isotropic particle distributions. This particular study is performed based on the transverse spherocity variable known to be sensitive to the transverse event shape [32–34], which gives information on how the particles are distributed perpendicularly to the collision axis.

This paper presents measurements of event-by-event fluctuations of the event-wise mean transverse momentum, $\langle p_T \rangle$, of charged particles produced in pp collisions at $\sqrt{s} = 5.02$ TeV, Xe–Xe collisions at $\sqrt{s_{NN}} = 5.44$ TeV, and Pb–Pb collisions at $\sqrt{s_{NN}} = 5.02$ TeV as a function of charged-particle multiplicity recorded using the ALICE detector at the LHC. The primary goal of the measurements is to examine how the strength of the $\langle\langle \Delta p_T \Delta p_T \rangle\rangle$ correlator evolves with the collision energy by comparing to previous results from Pb–Pb collisions at $\sqrt{s} = 2.76$ TeV and the collision system size, and determine whether this evolution can be understood quantitatively based on existing models. Additionally, since the presence of jet constituents is likely to influence the magnitude of the measured correlations, particularly in small collision systems, this work also includes an analysis of the strength of the $\langle\langle \Delta p_T \Delta p_T \rangle\rangle$ correlator in pp collisions based on the transverse shape of events (discussed in Sec. 2.3).

The paper is organized as follows: Sec. 2 presents a summary of the techniques used to evaluate the transverse momentum correlator $\langle\langle \Delta p_T \Delta p_T \rangle\rangle$ and derived quantities used in this work. It also includes a short discussion of the definition and techniques used towards measurements of the evolution of the $\langle\langle \Delta p_T \Delta p_T \rangle\rangle$ correlation strength with the transverse event shape in pp collisions. Details of the experimental methods and techniques used to determine systematic uncertainties are discussed in Sec. 3. The main results are presented in Sec. 4 and compared with those of previous measurements and model predictions. The paper is concluded with a summary in Sec. 5.

2 Observable definitions

The formal definition of the $\langle\langle \Delta p_T \Delta p_T \rangle\rangle$ correlator in terms of two-particle density is introduced in Sec. 2.1. In this work, $\langle\langle \Delta p_T \Delta p_T \rangle\rangle$ is measured based on an event-wise estimator and the method of moments presented in Sec. 2.2. The transverse spherocity estimator is defined in Sec. 2.3.

2.1 Definition of $\langle\langle \Delta p_T \Delta p_T \rangle\rangle$

Nominally, studies of average p_T fluctuations are carried out based on the integral correlator $\langle\langle \Delta p_{T1} \Delta p_{T2} \rangle\rangle$ (see Refs. [26, 35, 36]) defined according to the following formula

$$\langle\langle \Delta p_{T1} \Delta p_{T2} \rangle\rangle \equiv \frac{\int \rho_2(p_{T1}, p_{T2}) \Delta p_{T1} \Delta p_{T2} dp_{T1} dp_{T2}}{\int \rho_2(p_{T1}, p_{T2}) dp_{T1} dp_{T2}}, \quad (1)$$

where $\rho_2(p_{T1}, p_{T2})$ represents a two-particle density. This function is expressed in terms of the transverse momenta p_{T1} and p_{T2} of two particles.

The term $\Delta p_{Ti} = p_{Ti} - \langle\langle p_T \rangle\rangle$, where $i = 1, 2$, represents the transverse momentum deviates of particles 1 and 2, of a given pair, relative to the inclusive average $\langle\langle p_T \rangle\rangle$. The inclusive average $\langle\langle p_T \rangle\rangle$ is defined

according to

$$\langle\langle p_T \rangle\rangle \equiv \frac{\int \rho_1(p_T) p_T dp_T}{\int \rho_1(p_T) dp_T}, \quad (2)$$

in which $\rho_1(p_T)$ is the inclusive single-particle density.

2.2 Measurement method

The measurements of $\langle\langle \Delta p_{T1} \Delta p_{T2} \rangle\rangle$ are obtained based on an event-wise statistical estimator [22, 36] defined according to

$$\langle\langle \Delta p_{T1} \Delta p_{T2} \rangle\rangle = \left\langle \frac{\sum_{i,j=1; i \neq j}^{N_{ch}} (p_{Ti} - \langle\langle p_T \rangle\rangle)(p_{Tj} - \langle\langle p_T \rangle\rangle)}{N_{ch}(N_{ch}-1)} \right\rangle, \quad (3)$$

with the event-wise average transverse momentum

$$\langle\langle p_T \rangle\rangle = \frac{1}{N_{ch}} \sum_{i=1}^{N_{ch}} p_{Ti}. \quad (4)$$

In these equations, N_{ch} represents the total number of charged particles measured within a single event, and p_{Ti} and p_{Tj} denote the transverse momenta of the i^{th} and j^{th} particles, respectively, with $i, j = 1, \dots, N_{ch}$, and $i \neq j$ to avoid self-correlations. The average is said to be an event-wise average because the sum of the product of deviates is divided by the number of pairs of particles in each event. The angle bracket, $\langle\langle O \rangle\rangle$, represents the average of the event-wise observable $\langle O \rangle$ computed over an event ensemble of interest. In this analysis, values of the correlator $\langle\langle \Delta p_{T1} \Delta p_{T2} \rangle\rangle$ were determined for minimum bias event samples and for specific classes of the events selected based on their charged-particle multiplicity measured in forward and backward detectors (see Sec. 3). Additionally, the pp collisions were categorized into event subsets based on a measurement of their transverse spherocity defined in Sec. 2.3.

Computationally, it is advantageous to reformulate the analysis of $\langle\langle \Delta p_{T1} \Delta p_{T2} \rangle\rangle$ with the introduction of an event-wise variable Q_n defined according to

$$Q_n = \sum_{i=1}^{N_{ch}} (p_{Ti})^n, \quad (5)$$

where p_{Ti} represents the transverse momentum of particles, $i = 1, \dots, N_{ch}$, used in the measurement of $\langle\langle \Delta p_{T1} \Delta p_{T2} \rangle\rangle$. One verifies that $\langle\langle \Delta p_{T1} \Delta p_{T2} \rangle\rangle$ can be readily computed, according to [37], as

$$\langle\langle \Delta p_{T1} \Delta p_{T2} \rangle\rangle = \left\langle \frac{(Q_1)^2 - Q_2}{N_{ch}(N_{ch}-1)} \right\rangle - \left\langle \frac{Q_1}{N_{ch}} \right\rangle^2. \quad (6)$$

This analytic approach [37] simplifies the computations, thus significantly reducing the analysis time, especially in high-multiplicity events. In order to study the particle-density dependence of the correlator and minimize smearing effects associated with broad bin widths, the analysis is performed in narrow intervals of the charged-particle multiplicity detected at forward rapidity (i.e., the forward detector acceptance as described in Sec. 3).

In the absence of particle correlations, i.e., for purely Poissonian fluctuations of the event-wise $\langle p_T \rangle$, the correlator $\langle\langle \Delta p_{T1} \Delta p_{T2} \rangle\rangle$ vanishes. However, it acquires a finite value, either positive or negative, when the transverse momenta of the produced particles are correlated. Note that both the numerator and the denominator of $\langle\langle \Delta p_{T1} \Delta p_{T2} \rangle\rangle$ are proportional to the square of the particle detection efficiency making $\langle\langle \Delta p_{T1} \Delta p_{T2} \rangle\rangle$ robust against particle losses [22], i.e., efficiencies approximately cancel out in measurements of $\langle\langle \Delta p_{T1} \Delta p_{T2} \rangle\rangle$. However, the cancellation is not perfect, particularly if the detection efficiency depends on the p_T of particles.

The $\langle\langle \Delta p_{T1} \Delta p_{T2} \rangle\rangle$ correlator measures particle momentum correlations based on deviations relative to the mean momentum. In heavy-ion collisions, the mean momentum is known to depend in part on collective effects and more particularly, radial flow [38]. One thus expects $\langle\langle \Delta p_{T1} \Delta p_{T2} \rangle\rangle$ to depend on the magnitude of radial flow. This dependence can be largely suppressed by formulating the results in terms of the dimensionless quantity $\sqrt{\langle\langle \Delta p_{T1} \Delta p_{T2} \rangle\rangle / \langle p_T \rangle}$, indicated as the normalized transverse momentum correlator. The use of a dimensionless observable features a number of additional advantages: independence from uncertainties on the momentum scale, partial independence from the magnitude of $\langle p_T \rangle$, and further reduction of sensitivity to the dependence of the particle detection and reconstruction efficiency on the transverse momentum [22]. The results reported here are thus presented in terms of $\sqrt{\langle\langle \Delta p_{T1} \Delta p_{T2} \rangle\rangle / \langle p_T \rangle}$, in lieu of $\langle\langle \Delta p_{T1} \Delta p_{T2} \rangle\rangle$. Note that at variance with prior notations [17], the double bracket notation is used to clearly denote that the correlator is measured as an event ensemble average of the average pair-wise $\Delta p_T \Delta p_T$ measured event-by-event. The measurement carried out in this work is otherwise equivalent to those reported earlier in Ref. [22].

2.3 Definition of the transverse spherocity

In small collision systems, particularly in pp collisions, the many specific processes contributing to particle production have varying (fluctuating) contributions from one collision to another. Some collisions may thus feature sizable contributions from minijets (created by hard QCD scatterings at intermediate p_T) or jets, while others may be dominated by “soft” multipartonic interactions. Given that, on average, these processes feature different momentum scales and produced multiplicities, it is of interest to examine the relative role they play in influencing the strength of the $\langle\langle \Delta p_{T1} \Delta p_{T2} \rangle\rangle$ correlator. This is accomplished by further classifying pp collisions based on their transverse shape estimated with the transverse spherocity observable, S_0 [33].

The observable, S_0 , is defined according to

$$S_0 = \frac{\pi^2}{4} \min_{\hat{n}=(n_x, n_y, 0)} \left(\frac{\sum_{i=1}^{N_{ch}} \hat{p}_{T_i} \times \hat{n}}{\sum_{i=1}^{N_{ch}} \hat{p}_{T_i}} \right)^2, \quad (7)$$

where \hat{p}_{T_i} represents transverse momentum unit vectors. The orientation of \hat{n} , a two-dimensional unit vector of momentum in the transverse (xy) plane, perpendicular to the beam axis, is chosen such that S_0 is minimized on an event-by-event basis. By construction, S_0 ranges from 0 for pencil-like (jetty) events to a maximum of 1 for circularly symmetric events in the transverse plane, i.e., transversely isotropic events. For this analysis, the p_T -unweighted definition of transverse spherocity ($p_T = 1$) is used to quantify the topology in the azimuthal plane [39].

3 Data analysis

The data samples used in this analysis were collected by the ALICE experiment during the data-taking periods with pp collisions at $\sqrt{s} = 5.02$ and 13 TeV in 2015, Pb–Pb collisions at $\sqrt{s_{NN}} = 5.02$ TeV in 2015, and Xe–Xe collisions at $\sqrt{s_{NN}} = 5.44$ TeV in 2017. The data were acquired with a minimum bias trigger requiring coincident signals in the two scintillator arrays of the V0 detector covering forward (V0A, $2.8 < \eta < 5.1$) and backward (V0C, $-3.7 < \eta < -1.7$) pseudorapidity intervals. The V0 detector helps to reject the beam-induced background via V0 timing cuts. Detailed descriptions of the ALICE detectors, its components, and their performance, have been reported in Refs. [40, 41].

Charged-particle multiplicities measured with the V0 detectors were additionally used to divide the measured datasets into several multiplicity classes expressed as percentiles of the total hadronic cross section: eleven in Pb–Pb [42] and Xe–Xe [43] collisions, and nine in pp collisions. These classes were used to

characterize the $\langle p_T \rangle$ fluctuations with respect to the produced charged-particle multiplicity in pp collisions. In heavy-ion collisions, the charged-particle multiplicity is related to the impact parameter, which is the distance in the transverse plane between the centers of the colliding nuclei, of Xe–Xe and Pb–Pb collisions.

Measurements of $\langle p_T \rangle$ fluctuations were based on charged-particle tracks reconstructed with the ITS and the Time Projection Chamber (TPC). The analysis was further restricted to particles emitted within the pseudorapidity range $|\eta| < 0.8$ and the transverse momentum range $0.15 < p_T < 2 \text{ GeV}/c$. The selection on p_T is designed to focus the analysis of soft particle production in the “bulk” while minimizing contributions from the fragmentation of jets. The pseudorapidity range is selected to ensure uniform particle detection efficiency.

The events with a reconstructed primary vertex within 10 cm of the nominal interaction point along the beam direction ($|V_z| < 10 \text{ cm}$) are chosen to ensure uniform acceptance in pseudorapidity in $|\eta| < 0.8$ for the ITS. Additionally, events were considered in the analysis if at least one accepted charged particle contributed to the reconstruction of the primary vertex. Furthermore, events featuring more than one reconstructed primary interaction vertex were rejected to suppress the possibility of event pile-up. In all, 13 million, 1.4 million, and 104 million events passed the above criteria and were retained towards the analysis of $\langle p_T \rangle$ fluctuations from Pb–Pb, Xe–Xe, and pp ($\sqrt{s} = 5.02 \text{ TeV}$) collisions, respectively.

Individual charged-particle tracks were also subjected to track-quality selection criteria and to specific selections to limit the analysis to primary particles, i.e., particles with a mean proper lifetime τ larger than $1 \text{ cm}/c$, which are either produced directly in the interaction, or from decays of particles with τ smaller than $1 \text{ cm}/c$, restricted to decay chains leading to the interaction [44]. In pp collisions, the analysis was limited to charged tracks with a minimum of $N_{\text{TPC}} = 70$ reconstructed space points in the TPC, out of a maximum of 159, whereas in Pb–Pb and Xe–Xe collisions, a p_T -dependent cut, $N_{\text{TPC}} = 70 + 1.5 \times \frac{p_T}{\text{GeV}/c}$, was applied to further limit the probability of split tracks which is more relevant for events with high hit occupancy in the TPC. This occurs when a single particle is reconstructed as multiple separate tracks. Additionally, in order to suppress secondary charged particles, the track distance-of-closest-approach (DCA) to the reconstructed primary interaction vertex was limited to $|d_z| < 1 \text{ cm}$ in the longitudinal direction and $|d_{xy}| < 1 \text{ cm}$ in the transverse direction in Pb–Pb and Xe–Xe collisions. Finally, the DCA selection criteria, $|d_z| < 2 \text{ cm}$ and $|d_{xy}| < 0.0182 + 0.0350/p_T^{1.01} \text{ cm}$, with p_T expressed in units of GeV/c were used to minimize contamination from secondary particles in pp collisions [45].

Charged particles selected for the determination of S_0 were measured within the TPC and the ITS and required to have transverse momentum $p_T > 0.15 \text{ GeV}/c$ and lie within the pseudorapidity interval $|\eta| < 0.8$. The event shape-dependent analysis was further restricted to events featuring a minimum of five charged particles, $N_{\text{ch}} \geq 5$, to ensure that the notion of transverse topology (a.k.a. transverse event shape) is meaningful. The analysis of $\langle\langle \Delta p_{T1} \Delta p_{T2} \rangle\rangle$ was carried out as a function of the strength of S_0 and is reported for jetty events and isotropic events, based on two spherocity event classes corresponding to the lowest and top 20 percentile of all accepted events, respectively.

A comprehensive analysis was conducted to understand the impact of the detector response and analysis procedure on the measured observables, utilizing simulations based on different Monte Carlo event generators and on the GEANT3 [46] transport code, including a detailed description of the ALICE detector components and their performance. Observables of interest were computed at the generator level, i.e., directly based on the output of event generators, and at the detector level, i.e., based on the output of the reconstruction of simulated events. Ratios of the detector-level and generator-level results were considered in what is known as a closure test. The generator level computation involves no particle losses and no resolution smearing, whereas the reconstructed level includes both losses and smearing effects, as well as potential sources of contamination of the signal (poorly reconstructed tracks, tracks resulting from secondary particles, etc.). The event generators used for the MC closure tests were HIJING [47]

for Pb–Pb and Xe–Xe collisions, and PYTHIA8 [48] for pp collisions. From the analysis of the closure test, it was found that the detector-level results matched those obtained at the generator level within 2%. This difference was assigned as a systematic uncertainty, as discussed in Sec. 3.1.

The overall good closure obtained from the simulated data indicates, in particular, that the observable $\sqrt{\langle\langle \Delta p_{T1} \Delta p_{T2} \rangle\rangle} / \langle p_T \rangle$ is robust against particle losses and the analysis reported thus does not include corrections for such losses.

In addition to HIJING and PYTHIA 8, the AMPT [49] and EPOS LHC [50] models were used to compute the magnitude of the $\sqrt{\langle\langle \Delta p_{T1} \Delta p_{T2} \rangle\rangle} / \langle p_T \rangle$ correlator and its evolution with collision centrality in Xe–Xe and Pb–Pb collisions to provide insight into the interpretation of the data. The subsequent paragraphs provide a succinct overview of the models utilized for the different collision systems.

AMPT is a heavy-ion collision model that features partonic scattering and string fragmentation components in addition to a transport model. It has had considerable successes in reproducing observables measured in heavy-ion collisions at both RHIC and LHC energies, such as the strength of anisotropic flow harmonics [49, 51]. However, it has encountered mitigated success in the prediction of correlation and fluctuation observables [52]. The data presented in this paper will enable further testing of the underlying physics hypotheses of the model. AMPT simulations were performed with default and string melting settings. In the default mode, the model assumes that hadrons are produced directly from strings via Lund string fragmentation whereas in the string melting mode, the model melts these strings into their constituent partons. Thus, all produced hadrons are decomposed into partons immediately after their formation. After the partonic phase, partons recombine to form hadrons through quark coalescence.

HIJING is a perturbative QCD inspired MC event generator for the study of jet and multiparticle production in high-energy pp and heavy-ion collisions. The model includes multi-minijet production, nuclear shadowing of parton distribution functions, and mechanisms of jet interactions in a dense medium. In this analysis, HIJING simulations are used for comparisons with results from heavy-ion collisions.

PYTHIA is a MC event generator designed to simulate high-energy collisions between electrons, protons, photons, and heavy-nuclei. It features hard and soft interactions, sampling of parton distributions, initial- and final-state parton showers, multiparton interactions, as well as fragmentation and decays. Two tunes of PYTHIA are used in this analysis. PYTHIA 6 Perugia 2011 includes the revised set of parameters of flavor and fragmentation, which improves the overall description of Tevatron data and the reliability of their extrapolations to LHC energies [53]. The minimum bias and underlying event data from the LHC are taken into account in Perugia 2011 tune. PYTHIA 8 Monash tune includes a default parameterization of the model based on multiparton interactions and color reconnection mechanism. Following the hard scattering and parton showers, colored strings are formed with the final-state partons. PYTHIA 8 has a hadronization mechanism based on the fragmentation model which is followed by particle decays, which leads to the production of jets and the underlying event [48].

The EPOS LHC model features particle production from core and corona components. Particle production in the corona is described in the context of the Parton-Based Gribov–Regge theory, whereas the core, expected to feature high parton densities, is described with ideal hydrodynamics. EPOS LHC is tuned to the LHC data via the color exchange mechanism of string excitation [54].

3.1 Systematic uncertainties

Several potential sources of systematic uncertainties were considered including effects due to collision pile-up, contributions from tracks reconstructed with limited precision, secondary tracks, non-uniformity of the acceptance, and possible dependencies of the track reconstruction efficiency on the position of the primary vertex. Testing for these contributions was accomplished by studying the magnitude of the $\sqrt{\langle\langle \Delta p_{T1} \Delta p_{T2} \rangle\rangle} / \langle p_T \rangle$ correlator in response to variations of event and track quality selection criteria used in the analysis and also by comparing different data subsets. The systematic uncertainty for each

source was determined based on the maximum difference between the results obtained with the default analysis configuration and with the different variations of the selection criteria.

At the event level, the selections on the reconstructed position of the primary vertex along the beam axis (V_z), and on the presence of multiple reconstructed primary vertices to suppress events with collision pile-up were varied. The V_z selection is varied to $|V_z| < 8$ cm and contributes to relative uncertainties smaller than 2.1% for pp collisions, 3.7% for Xe–Xe collisions, and 2.2% in Pb–Pb collisions. The relative uncertainties due to remaining pile-up contamination are less than 2% and 3.3% for pp and Xe–Xe collisions, respectively, and vary from a minimum of 0.1% to a maximum 3.5% for Pb–Pb collisions. At the track level, the track-quality and primary-particle selection criteria were varied including the longitudinal and transverse DCA of each track and the minimum number of TPC clusters required on a track. The maximum contribution to the systematic uncertainty due to the track selection criteria arises from the d_z selection, and it is less than 5.5%, 3.1%, and 0.8%, in pp, Xe–Xe, and Pb–Pb collisions, respectively. Other relevant contributions to the systematic uncertainty on the track selection are due to the d_{xy} cut (up to 4% in pp collisions), the d_z cut (up to 5.5% in pp collisions), and the request of a minimum number of TPC clusters (up to 2.2% in Xe–Xe collisions). The analysis of the closure test results showed that deviations between detector and generator levels do not exceed 2% in all studied collision systems. The minor deviations from perfect closure are conservatively added to the systematic uncertainties. The estimated values of the relative systematic uncertainties for the three collision systems are summarized in Table 1. For the sources of uncertainty that depend on multiplicity a range of values is reported. Individual contributions are summed in quadrature to obtain the total systematic uncertainties. The total systematic uncertainties are smaller than 7.1%, 6.7%, and 3.8% for pp, Xe–Xe and Pb–Pb collisions, respectively.

Table 1: Contributions to the relative (%) systematic uncertainty on $\sqrt{\langle\langle \Delta p_{T1} \Delta p_{T2} \rangle\rangle / \langle\langle p_T \rangle\rangle}$ of primary charged particles in pp and Pb–Pb collisions at $\sqrt{s_{NN}} = 5.02$ TeV and Xe–Xe collisions at $\sqrt{s_{NN}} = 5.44$ TeV.

Source of uncertainty	pp, 5.02 TeV	Xe–Xe, 5.44 TeV	Pb–Pb, 5.02 TeV
Vertex selection	< 2.1%	< 3.7%	< 2.2%
Pile-up	< 2.0%	< 3.3%	0.1–3.5%
No. of TPC clusters	0.1–2.0%	< 2.2%	< 0.5%
d_{xy}	0.2–4.0%	< 1.5%	< 0.3%
d_z	3.1–5.5%	< 3.1%	< 0.8%
MC closure	1.3%	1.8%	1.5%
Total	4.0–7.1%	1.8–6.7%	2.2–3.8%

4 Results

Results of the study of the dependence of the magnitude of the $\sqrt{\langle\langle \Delta p_{T1} \Delta p_{T2} \rangle\rangle / \langle\langle p_T \rangle\rangle}$ correlator on the produced particle density measured in pp, Xe–Xe, and Pb–Pb collision systems are presented in Sec. 4.1. The comparison of the measurements to theoretical predictions, and the energy dependence of the correlator are discussed in Secs. 4.2 and 4.3, respectively. The dependence of the $\sqrt{\langle\langle \Delta p_{T1} \Delta p_{T2} \rangle\rangle / \langle\langle p_T \rangle\rangle}$ on the event spherocity S_0 measured in pp collisions is discussed in Sec. 4.4

4.1 System size dependence of event-by-event $\langle p_T \rangle$ fluctuations

The event-by-event $\langle p_T \rangle$ fluctuations is reported based on the two-particle correlator $\sqrt{\langle\langle \Delta p_{T1} \Delta p_{T2} \rangle\rangle / \langle\langle p_T \rangle\rangle}$ defined in Eq. (1) and computed according to Eq. (3). The top panel of Fig. 1 presents the magnitude of $\sqrt{\langle\langle \Delta p_{T1} \Delta p_{T2} \rangle\rangle / \langle\langle p_T \rangle\rangle}$ measured as a function of the pseudorapidity density of charged particles produced in the collision, $\langle dN_{ch}/d\eta \rangle$, determined in the kinematic range $0.15 < p_T < 2$ GeV/c and $|\eta| < 0.8$, in pp collisions at $\sqrt{s} = 5.02$ TeV, Xe–Xe collisions at $\sqrt{s_{NN}} = 5.44$ TeV, and Pb–Pb collisions at $\sqrt{s_{NN}} =$

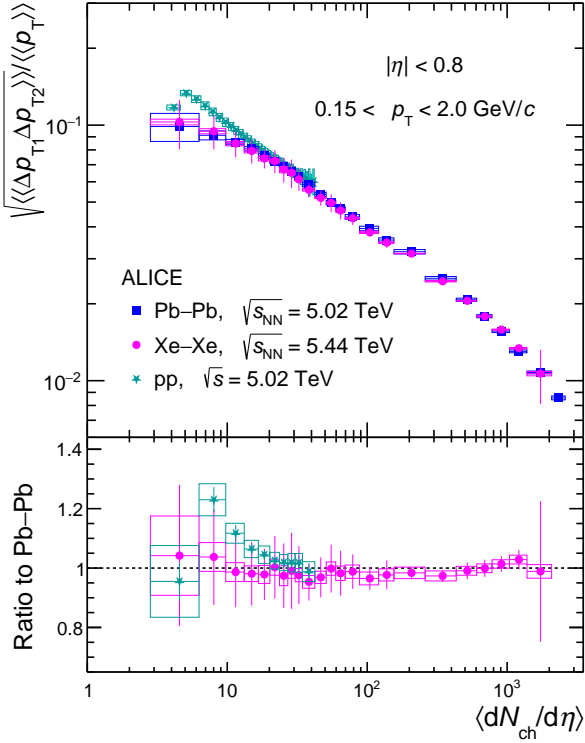


Figure 1: (top) Normalized transverse momentum correlator, $\sqrt{\langle\langle \Delta p_{T1} \Delta p_{T2} \rangle\rangle / \langle\langle p_T \rangle\rangle}$, shown as a function of the charged-particle multiplicity density, $\langle dN_{ch}/d\eta \rangle$, measured in the pseudorapidity range $|\eta| < 0.8$ in pp collisions at $\sqrt{s} = 5.02 \text{ TeV}$, Xe–Xe collisions at $\sqrt{s_{NN}} = 5.44 \text{ TeV}$, and Pb–Pb collisions at $\sqrt{s_{NN}} = 5.02 \text{ TeV}$; (bottom) Ratio of values of $\sqrt{\langle\langle \Delta p_{T1} \Delta p_{T2} \rangle\rangle / \langle\langle p_T \rangle\rangle}$ measured in pp and Xe–Xe collisions to those observed in Pb–Pb collisions. Statistical and systematic uncertainties are represented by vertical bars and boxes, respectively.

5.02 TeV. The strength of $\sqrt{\langle\langle \Delta p_{T1} \Delta p_{T2} \rangle\rangle / \langle\langle p_T \rangle\rangle}$ is evidently non-vanishing and exhibits an approximate power-law dependence on the produced charged-particle density. Fluctuations of the event-wise average momentum $\langle p_T \rangle$ are accordingly non-Poissonian and exhibit a strong dependence on the particle density in all three collision systems studied. These new results confirm and corroborate prior observations of non-Poissonian fluctuations in heavy-ion collisions and make it possible to carry out a detailed study of the system size and energy dependence of the fluctuations [11–13, 17, 18, 22, 55, 56].

The correlator strength is observed to decrease by more than one order of magnitude with increasing multiplicity for Xe–Xe and Pb–Pb collisions. One notes, however, that this multiplicity dependence cannot be described by a single power-law across the whole range of $\langle dN_{ch}/d\eta \rangle$. One finds, indeed, that in both Pb–Pb (blue square) and Xe–Xe (magenta circle) collisions, the dependence can be characterized by three power-law regimes with distinct slopes in the ranges $3 < \langle dN_{ch}/d\eta \rangle < 20$, $20 < \langle dN_{ch}/d\eta \rangle < 300$, and $\langle dN_{ch}/d\eta \rangle > 300$, respectively. This suggests that the strength of the correlation is influenced by several distinct mechanisms (or system properties) from the most peripheral to the most central collisions considered in this study, as discussed in more detail in the following.

The lower panel of Fig. 1 displays the evolution of the ratio of the correlation strength measured in pp and Xe–Xe collisions relative to that observed in Pb–Pb collisions at $\sqrt{s_{NN}} = 5.02 \text{ TeV}$. To compute the ratio, the pp and Xe–Xe results were rebinned to the $\langle dN_{ch}/d\eta \rangle$ intervals used for Pb–Pb results, using a fit function. It is apparent that the magnitude of the correlators measured in Pb–Pb and Xe–Xe are consistent between each other and feature essentially the same dependence on $\langle dN_{ch}/d\eta \rangle$. By contrast, however, the evolution of the correlator strength measured in pp collisions differs from that observed in

the larger systems. Nevertheless, in pp collisions at the higher values (>20) of particle multiplicities, $\langle dN_{ch}/d\eta \rangle$, the correlator strength is in very good agreement, within statistical uncertainties, to that reported in Pb–Pb and Xe–Xe at the same particle density. For decreasing $\langle dN_{ch}/d\eta \rangle$ the correlation strength measured in pp progressively deviates from the values observed for the larger systems. Overall, one finds that the evolution of $\sqrt{\langle\langle \Delta p_{T1} \Delta p_{T2} \rangle\rangle / \langle\langle p_T \rangle\rangle}$ with $\langle dN_{ch}/d\eta \rangle$ follows similar trends in Pb–Pb and Xe–Xe whereas pp interactions reveals discrepancies at low multiplicities.

4.2 Comparison to theoretical predictions

Figure 2 shows the comparison of the evolution of the measured $\sqrt{\langle\langle \Delta p_{T1} \Delta p_{T2} \rangle\rangle / \langle\langle p_T \rangle\rangle}$ as a function of $\langle dN_{ch}/d\eta \rangle$ in Pb–Pb (left) and Xe–Xe (right) collisions with the results obtained using HIJING and AMPT models. The presented AMPT calculations were obtained for two scenarios: AMPT default and AMPT string melting.

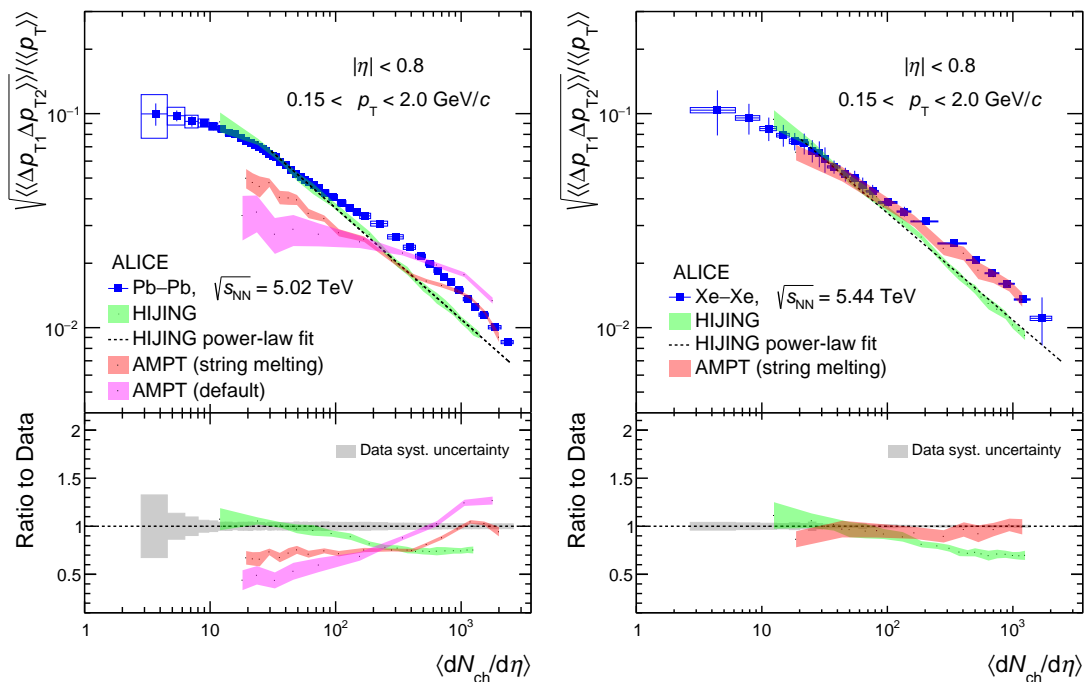


Figure 2: Upper panels: Comparisons of the evolution of the strength of $\sqrt{\langle\langle \Delta p_{T1} \Delta p_{T2} \rangle\rangle / \langle\langle p_T \rangle\rangle}$ with produced charged-particle multiplicity densities, $\langle dN_{ch}/d\eta \rangle$, in Pb–Pb collisions at $\sqrt{s_{NN}} = 5.02$ TeV (left) and Xe–Xe collisions at $\sqrt{s_{NN}} = 5.44$ TeV (right) with calculations using the HIJING and AMPT models. Lower panels: Ratios of the model calculations to measured $\sqrt{\langle\langle \Delta p_{T1} \Delta p_{T2} \rangle\rangle / \langle\langle p_T \rangle\rangle}$. Solid symbols represent the measured data with statistical (vertical bars) and systematic (boxes) uncertainties. Model calculations are shown with shaded bands denoting their statistical uncertainty.

The bottom panels of Fig. 2 show ratios of HIJING and AMPT calculations to the measured data. The observed magnitude of the normalized transverse momentum correlator, $\sqrt{\langle\langle \Delta p_{T1} \Delta p_{T2} \rangle\rangle / \langle\langle p_T \rangle\rangle}$, obtained with the HIJING model exhibits a simple power-law dependence. This behavior is accurately depicted by a fit of $\sqrt{\langle\langle \Delta p_{T1} \Delta p_{T2} \rangle\rangle / \langle\langle p_T \rangle\rangle} \propto \langle dN_{ch}/d\eta \rangle^\alpha$ where the exponent α is determined to be -0.504 ± 0.007 within the charged particle multiplicity density interval of $20 < \langle dN_{ch}/d\eta \rangle < 2500$.

This power-law dependence and the exponent value are consistent with the behavior expected for a system consisting of a simple superposition of nucleon–nucleon collisions without rescattering of the secondaries as modeled by HIJING. One finds, however, that while the evolution of the correlator mea-

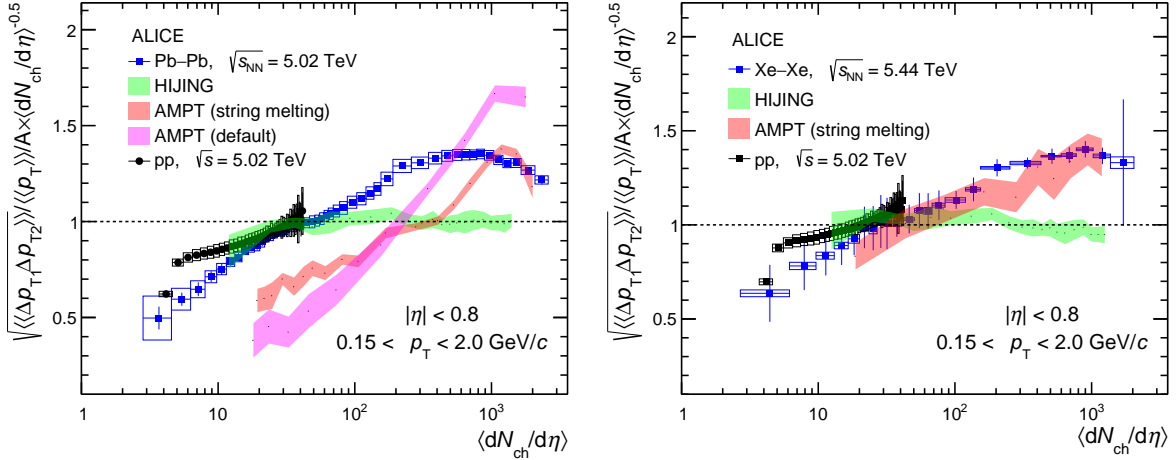


Figure 3: Evolution of the ratio of $\sqrt{\langle\langle \Delta p_{T1} \Delta p_{T2} \rangle\rangle} / \langle p_T \rangle$ to results of a power-law fit to HIJING calculations: (left) pp and Pb–Pb collisions at $\sqrt{s_{NN}} = 5.02$ TeV; (right) pp collisions at $\sqrt{s_{NN}} = 5.02$ TeV and Xe–Xe collisions at $\sqrt{s_{NN}} = 5.44$ TeV. The power-law fit was performed on correlator values obtained with HIJING for Pb–Pb collisions at $\sqrt{s_{NN}} = 5.02$ TeV and Xe–Xe collisions at $\sqrt{s_{NN}} = 5.44$ TeV for left and right panel, respectively, as described in the text. Solid symbols represent the measured data reported in this work with statistical (vertical bars) and systematic (boxes) uncertainties. Calculations of the ratios obtained with HIJING and AMPT calculations are shown with shaded bands denoting their statistical uncertainty.

sured in both Pb–Pb and Xe–Xe approximately follows the HIJING power-law fit in the low-multiplicity range $10 < \langle dN_{ch}/d\eta \rangle < 50$, it clearly deviates from this simple trend at $\langle dN_{ch}/d\eta \rangle > 50$. This is also highlighted in Fig. 3 that shows the ratio of the magnitude of the $\sqrt{\langle\langle \Delta p_{T1} \Delta p_{T2} \rangle\rangle} / \langle p_T \rangle$ correlator in Pb–Pb collisions at $\sqrt{s_{NN}} = 5.02$ TeV (left) and in Xe–Xe collisions at $\sqrt{s_{NN}} = 5.44$ TeV (right) to the power-law fit of $\langle p_T \rangle$ fluctuations of HIJING model. This indicates that the final-state particle production in Pb–Pb collisions at $\sqrt{s_{NN}} = 5.02$ TeV and Xe–Xe at $\sqrt{s_{NN}} = 5.44$ TeV cannot be described by a mere superposition of independent particle-emitting sources. It also corroborates the earlier findings by the ALICE Collaboration in Pb–Pb collisions at $\sqrt{s_{NN}} = 2.76$ TeV [22] and those of the STAR Collaboration at RHIC energies [17–19].

Deviations from a superposition model of independent particle-emitting sources, in A–A collisions, are known to arise in measurements of nuclear modification factor [45], and anisotropic flow [57], and other measurements of two-particle correlation functions [55, 58]. It is thus reasonable to seek theoretical guidance from a model such as AMPT, which has had relative success in the description of data obtained at RHIC and LHC. One finds that the two versions of AMPT considered strongly under-predict the strength of the $\sqrt{\langle\langle \Delta p_{T1} \Delta p_{T2} \rangle\rangle} / \langle p_T \rangle$ correlator in the most peripheral Pb–Pb collisions. The AMPT with string melting on, shows agreement with the data for Pb–Pb and Xe–Xe collisions in the high-multiplicity regions. However, it is evident that both HIJING and AMPT lack some important features that determine the strength and evolution of $\sqrt{\langle\langle \Delta p_{T1} \Delta p_{T2} \rangle\rangle} / \langle p_T \rangle$ with collision centrality. For Xe–Xe collisions, AMPT with string melting on, shows a better agreement with data than for Pb–Pb collisions for low multiplicity region.

In order to guide further theoretical inquiries, the strength and evolution of $\sqrt{\langle\langle \Delta p_{T1} \Delta p_{T2} \rangle\rangle} / \langle p_T \rangle$ observed in pp, Pb–Pb and Xe–Xe collisions are compared in more detail.

Figure 3 shows the ratio of measured values of $\sqrt{\langle\langle \Delta p_{T1} \Delta p_{T2} \rangle\rangle} / \langle p_T \rangle$ to the HIJING results estimated by a power-law fit to the correlator values. Results are drawn as a function of the charged-particle multiplicity, $\langle dN_{ch}/d\eta \rangle$. The fitting procedure was carried over the range $25 < \langle dN_{ch}/d\eta \rangle < 2500$ with a

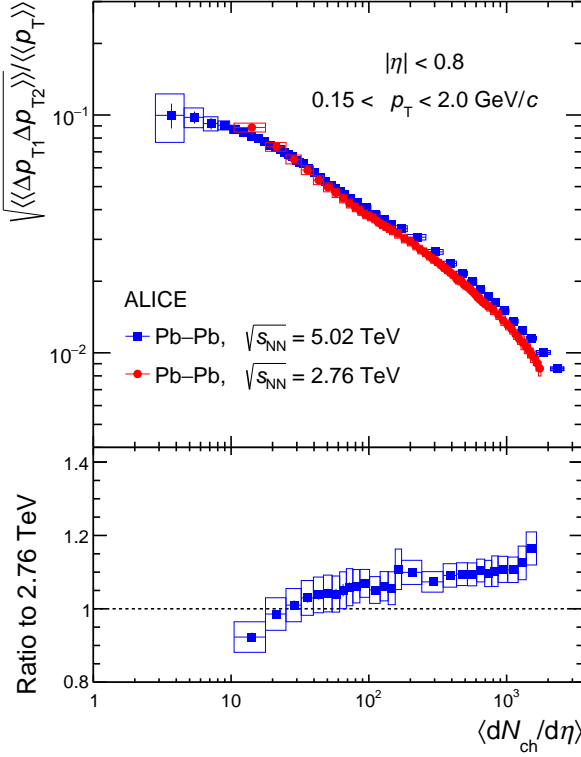


Figure 4: (top) Normalized transverse momentum correlator, $\sqrt{\langle\langle \Delta p_{T1} \Delta p_{T2} \rangle\rangle / \langle\langle p_T \rangle\rangle}$, shown as a function of the charged-particle multiplicity density, $\langle dN_{ch}/d\eta \rangle$, in Pb–Pb collisions at $\sqrt{s_{NN}} = 2.76$ [22] and 5.02 TeV; (bottom) Ratio of values of $\sqrt{\langle\langle \Delta p_{T1} \Delta p_{T2} \rangle\rangle / \langle\langle p_T \rangle\rangle}$ measured at $\sqrt{s_{NN}} = 5.02$ TeV to the corresponding results at $\sqrt{s_{NN}} = 2.76$ TeV. The statistical and systematic uncertainties for both energies are represented by vertical bars and boxes, respectively.

fixed exponent value of $\alpha = -0.5$. The shaded green band is approximately centered at unity and shows that the power-law fit is a good description of the evolution of the strength of $\sqrt{\langle\langle \Delta p_{T1} \Delta p_{T2} \rangle\rangle / \langle\langle p_T \rangle\rangle}$ with $\langle dN_{ch}/d\eta \rangle$ predicted by HIJING. Indeed, HIJING produces a progressive dilution of the correlator with rising values of $\langle dN_{ch}/d\eta \rangle$ as expected. By contrast, one finds that correlations observed in Pb–Pb and Xe–Xe increasingly undershoot the power-law fit at small densities while they significantly exceed the fit at $\langle dN_{ch}/d\eta \rangle$ above 70–80, thereby signaling a considerable departure from a system consisting of a superposition of independent nucleon–nucleon collisions. One additionally finds that both AMPT calculations considerably violate the density scaling. However, pp results exhibit scaling behavior at multiplicities greater than 10.

4.3 Energy dependence of event-by-event $\langle p_T \rangle$ fluctuations

Figure 4 shows the dependence of the correlator strength $\sqrt{\langle\langle \Delta p_{T1} \Delta p_{T2} \rangle\rangle / \langle\langle p_T \rangle\rangle}$ as a function of charged-particle multiplicity ($\langle dN_{ch}/d\eta \rangle$) for Pb–Pb collisions at two energies, $\sqrt{s_{NN}} = 2.76$ TeV and 5.02 TeV. The lower panel of the figure shows the ratio of 5.02 TeV correlator to that of 2.76 TeV. The ratio is close to unity at low values of $\langle dN_{ch}/d\eta \rangle$ and increases with increasing multiplicity. For central collisions (large values of $\langle dN_{ch}/d\eta \rangle$), the correlator at 5.02 TeV is up to 20% larger compared to the one at 2.76 TeV.

Fig. 5 (left panel) shows the dependence of the correlator as a function of the number of participant nucleons (N_{part}) for Pb–Pb collisions at two LHC energies and Au–Au collisions at $\sqrt{s_{NN}} = 200$ GeV at RHIC [17]. As shown in the ratio plot, the collision energy dependence in Pb–Pb collisions disappears

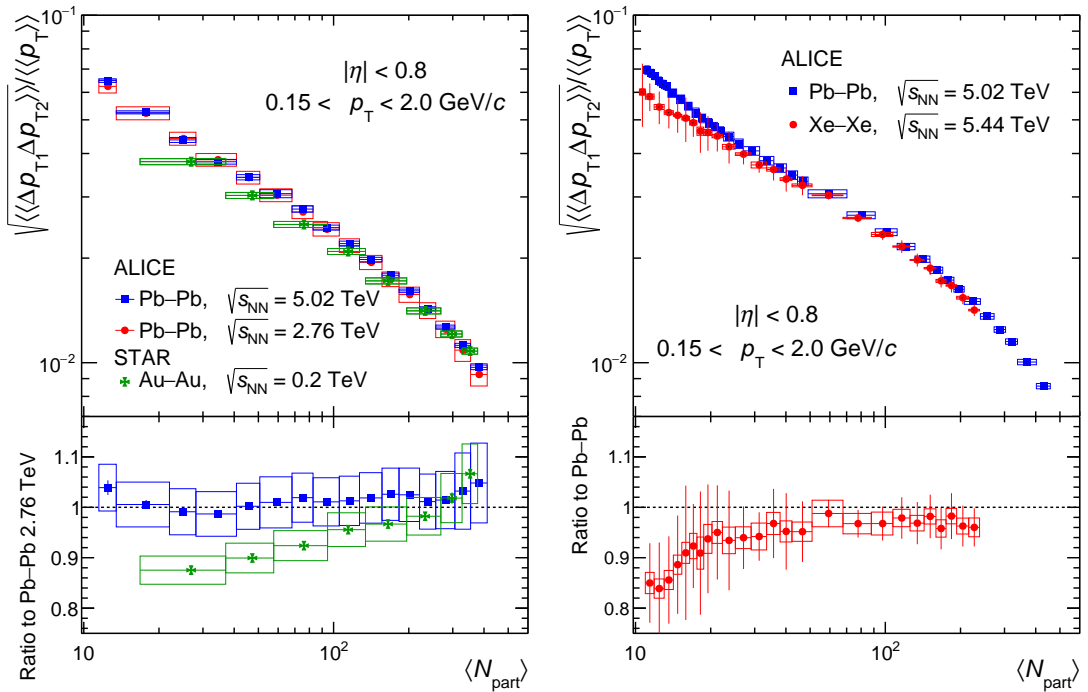


Figure 5: Left: Normalized transverse momentum correlator, $\sqrt{\langle\langle \Delta p_{T1} \Delta p_{T2} \rangle\rangle / \langle p_T \rangle}$, shown as a function of the average number of participant nucleons, $\langle N_{\text{part}} \rangle$, in Pb–Pb collisions at $\sqrt{s_{\text{NN}}} = 2.76$ and 5.02 TeV and Au–Au collisions at 0.2 TeV. right: Normalized transverse momentum correlator, $\sqrt{\langle\langle \Delta p_{T1} \Delta p_{T2} \rangle\rangle / \langle p_T \rangle}$, plotted as a function $\langle N_{\text{part}} \rangle$ in Xe–Xe collisions at $\sqrt{s_{\text{NN}}} = 5.44$ TeV and Pb–Pb collisions at $\sqrt{s_{\text{NN}}} = 5.02$ TeV. The statistical and systematic uncertainties are represented by vertical bars and boxes respectively.

when the correlator is shown as a function ($\langle N_{\text{part}} \rangle$). This suggests that for a given initial-state overlap geometry, the correlator strength is independent of the collision energy. However, an energy dependence is observed when comparing RHIC and LHC energies. The behavior in Fig. 4 could be due to the dependence of the $\langle p_T \rangle$ fluctuations on the collision energy or could be due to the larger number of particles produced at $\sqrt{s_{\text{NN}}} = 5.02$ TeV that shifts $\langle dN_{\text{ch}}/d\eta \rangle$ to a higher value as compared to $\sqrt{s_{\text{NN}}} = 2.76$ TeV. The energy dependence as a function of $\langle N_{\text{part}} \rangle$ in Fig. 5 corroborates with the above statement. The right panel of Fig. 5 shows that similar values of $\sqrt{\langle\langle \Delta p_{T1} \Delta p_{T2} \rangle\rangle / \langle p_T \rangle}$ are observed in Pb–Pb and Xe–Xe collisions for $\langle N_{\text{part}} \rangle > 25$ but differ by as much as 15% at smaller $\langle N_{\text{part}} \rangle$ (i.e. very peripheral collisions).

4.4 Transverse spherocity dependence of $\langle p_T \rangle$ fluctuations in pp collisions

The results in Fig. 3 indicate that the strength of the correlator in central Pb–Pb and Xe–Xe collisions deviates by as much as 30% from the trivial scaling expected in the dilution scenario of independent particle-emitting sources. Although this deviation might stem largely from the kinematic focusing of correlated pairs associated with radial flow, it is of interest to examine whether the enhanced correlation values might arise from fluctuations associated with jet production and, more particularly, event-by-event variations in the number of jets and their composition. One might naively expect that fluctuations in the number or constituents of jets relative to “baseline” collisions (with no jet) could increase fluctuations and thus change the magnitude of the correlator. It is thus interesting to investigate, based on pp collisions alone, how the magnitude of the correlator changes from collisions where effects of jets are less pronounced to those featuring prominent jets. This investigation is conducted by studying the magnitude of the $\sqrt{\langle\langle \Delta p_{T1} \Delta p_{T2} \rangle\rangle / \langle p_T \rangle}$ correlator relative to the shape of particle emission in the transverse plane. The spherocity observable, described in Sec. 2, is used to select collisions based on their transverse

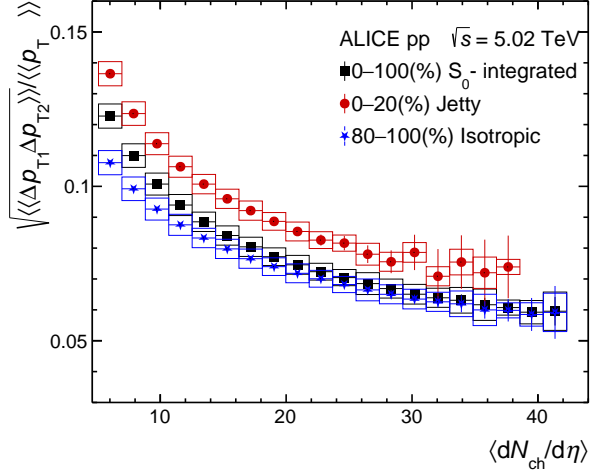


Figure 6: Comparison of the normalized transverse momentum correlator, $\sqrt{\langle\langle \Delta p_{T1} \Delta p_{T2} \rangle\rangle} / \langle p_T \rangle$ as a function of the charged-particle multiplicity density for spherocity-integrated (black), jetty (red), and isotropic (blue) events in pp collisions at $\sqrt{s} = 5.02$ TeV. The statistical and systematic uncertainties of the measured data for all spherocity classes are represented by vertical bars and boxes respectively.

shape. Collisions with $S_0 = 1$ are expected to feature few or no jets, as by construction these are isotropic events without any preferred direction. This can be also possible for events with multijets. Whereas, events with $S_0 \sim 0$ are expected to feature back-to-back jets. It is then nominally possible to get insight into the impact of jets on the magnitude of $\sqrt{\langle\langle \Delta p_{T1} \Delta p_{T2} \rangle\rangle} / \langle p_T \rangle$.

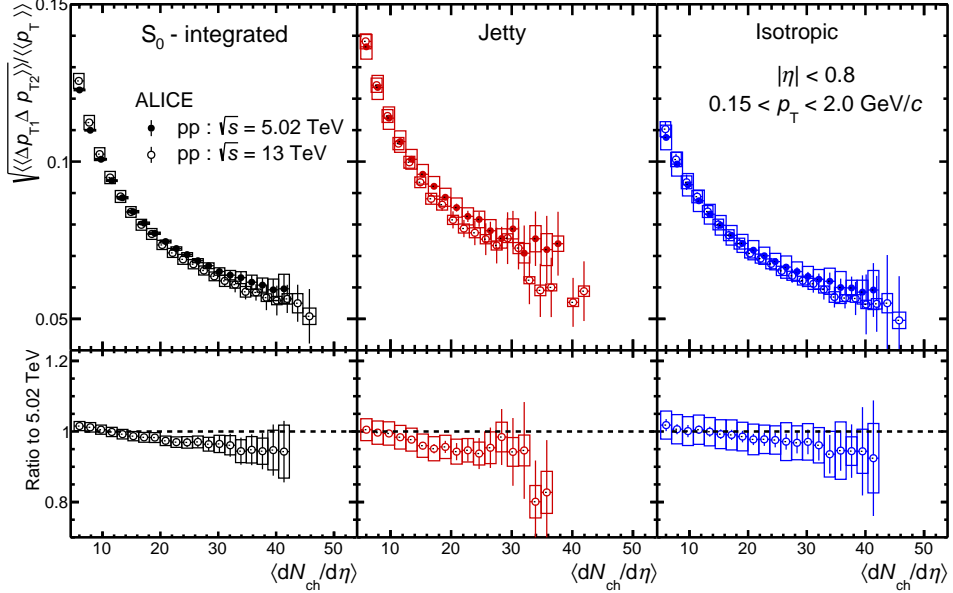


Figure 7: Upper panels: Comparison of the normalized transverse momentum correlator, $\sqrt{\langle\langle \Delta p_{T1} \Delta p_{T2} \rangle\rangle} / \langle p_T \rangle$ as a function of charged-particle density in pp collisions at $\sqrt{s} = 5.02$ and $\sqrt{s} = 13$ TeV for spherocity-integrated (left), jetty (middle) and isotropic (right) events; Lower panels: Ratio of the $\sqrt{\langle\langle \Delta p_{T1} \Delta p_{T2} \rangle\rangle} / \langle p_T \rangle$ in pp collisions at $\sqrt{s} = 13$ TeV to $\sqrt{s} = 5.02$ TeV. The statistical and systematic uncertainties of the measured data for all spherocity classes are represented by vertical bars and boxes, respectively.

Figure 6 presents measurements of the evolution of the strength of the correlator $\sqrt{\langle\langle \Delta p_{T1} \Delta p_{T2} \rangle\rangle} / \langle p_T \rangle$ as

a function of $\langle dN_{ch}/d\eta \rangle$ in pp collisions at $\sqrt{s} = 5.02$ TeV for selected spherocity classes. Black squares display inclusive events, i.e., events with no spherocity selection; red circles present events characterized by a back-to-back jet topology denoted as “jetty” in the following, with $S_0 < 0.425$ corresponding to the 20% of events with lower spherocity; and blue stars are for the 20% most isotropic events, with $S_0 > 0.745$. Low-spherocity events feature $\sqrt{\langle\langle \Delta p_{T1} \Delta p_{T2} \rangle\rangle / \langle\langle p_T \rangle\rangle}$ values larger than those observed for isotropic events. The presence of a pronounced back-to-back jet topology is found to enhance the magnitude of the correlator by about 20% in high-multiplicity collisions. This enhancement likely results from jet particles being emitted in a narrow cone and thus being more correlated on average than other particles. It is interesting to consider whether the observed 20% correlation strength difference between

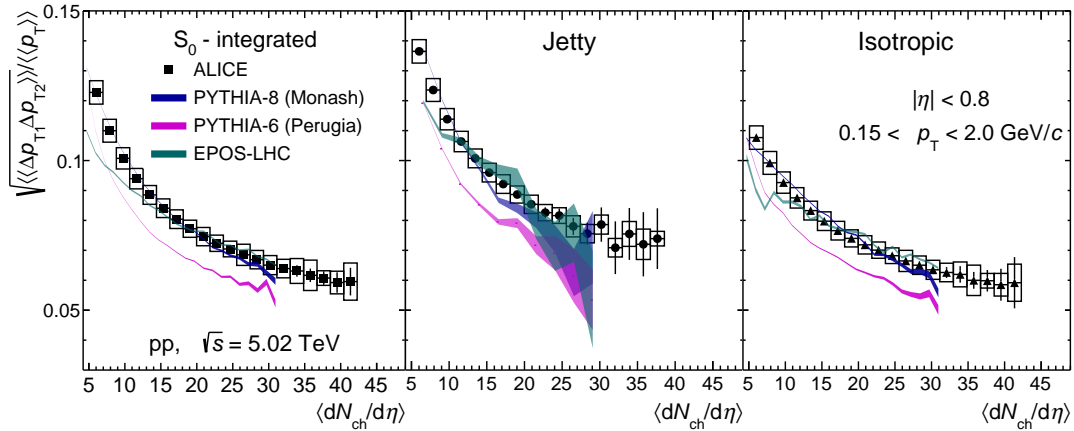


Figure 8: Comparison of normalized transverse momentum correlator, $\sqrt{\langle\langle \Delta p_{T1} \Delta p_{T2} \rangle\rangle / \langle\langle p_T \rangle\rangle}$ as a function of the produced particle multiplicity for integrated (left), jetty (middle), and isotropic (right) pp collisions at $\sqrt{s} = 5.02$ TeV with calculations from the PYTHIA and EPOS models. See text for details. The statistical and systematic uncertainties of the measured data for all spherocity classes are represented by vertical bars and boxes, respectively.

collisions dominated by a back-to-back jet topology and isotropic events may entail for correlation in larger systems. Since high- p_T particles and jets are suppressed in mid to central heavy-ion collisions, one expects that contributions to the $\sqrt{\langle\langle \Delta p_{T1} \Delta p_{T2} \rangle\rangle / \langle\langle p_T \rangle\rangle}$ correlator, from jet particles, might also be suppressed. This should then reduce the correlation strength relative to the scaled dependence resulting from the dilution of the correlator in mid to central heavy-ion collisions. However, note that an excess is observed relative to the scaled dependence in both Xe–Xe and Pb–Pb collisions. One can then infer that the excess of correlation strength observed in these systems is not likely linked to jets but rather arises from other causes. A possible cause of the increased strength may be the strong transverse radial flow arising from the rapid expansion of the matter formed in heavy-ion collisions [59–61]. Indeed, one expects that the transverse radial expansion should accelerate correlated particles resulting from resonance (high mass hadrons) decays, string fragmentation, or QGP hadronization, giving thus rise to larger $\sqrt{\langle\langle \Delta p_{T1} \Delta p_{T2} \rangle\rangle / \langle\langle p_T \rangle\rangle}$ correlator values.

It is also interesting to consider how the magnitude of $\sqrt{\langle\langle \Delta p_{T1} \Delta p_{T2} \rangle\rangle / \langle\langle p_T \rangle\rangle}$ evolves with \sqrt{s} in pp collisions. Figure 7 compares the dependence of $\sqrt{\langle\langle \Delta p_{T1} \Delta p_{T2} \rangle\rangle / \langle\langle p_T \rangle\rangle}$ on $\langle dN_{ch}/d\eta \rangle$ for inclusive, low- and high-spherocity events measured in pp collisions at $\sqrt{s} = 5.02$ TeV and 13 TeV. One observes the correlation strength exhibits only a small dependence, if any, on the energy of the pp collisions in both jetty and isotropic events. This indicates that changes in the strength of $\sqrt{\langle\langle \Delta p_{T1} \Delta p_{T2} \rangle\rangle}$ are essentially compensated by the rise in $\langle\langle p_T \rangle\rangle$ associated with the increase in the collision energy.

The measured $\langle p_T \rangle$ fluctuations for different spherocity classes are compared in Fig. 8 with calculations performed with the MC generators PYTHIA 6 [62], PYTHIA 8 [48], and EPOS LHC [54]. PYTHIA 6 significantly underestimates the magnitude of $\sqrt{\langle\langle \Delta p_{T1} \Delta p_{T2} \rangle\rangle / \langle\langle p_T \rangle\rangle}$, while PYTHIA 8 reproduces the

data rather well. This indicates that the MPI mechanism is crucial for the description of particle production in PYTHIA. In addition, EPOS LHC, a model with core-corona approach, also reproduces the data well in both spherocity classes.

5 Summary and conclusions

Event-by-event $\langle p_T \rangle$ fluctuations of charged particles produced in Pb–Pb and Xe–Xe collisions at $\sqrt{s_{\text{NN}}} = 5.02$ and 5.44 TeV, respectively, and in pp collisions at $\sqrt{s} = 5.02$ TeV are studied based on the normalized $\sqrt{\langle\langle \Delta p_{T1} \Delta p_{T2} \rangle\rangle} / \langle p_T \rangle$ integral correlator. The correlation strength is measured as a function of produced charged-particle multiplicity in all three collision systems and as a function of the spherocity of produced particles at midrapidity in pp collisions. The correlator strength is positive, thus indicating that significant dynamical fluctuations are observed in heavy-ion collisions and corroborating prior measurements reported by the STAR and ALICE Collaborations [61, 63]. The strength of $\sqrt{\langle\langle \Delta p_{T1} \Delta p_{T2} \rangle\rangle} / \langle p_T \rangle$ is also observed to monotonically decrease with increasing multiplicity in all measured systems, likely resulting in part from a dilution of the correlation strength associated with an increase in particle production. The observed decrease with multiplicity, however, significantly deviates from a power scaling of the form $\langle dN_{\text{ch}}/d\eta \rangle^{-1/2}$ expected for a source consisting of a superposition of independent nucleon–nucleon (or parton–parton) collisions with no re-scattering of the secondaries. A comparison of the correlation strength measured in low- and high-spherocity pp collisions shows that the selection of events characterized by a back-to-back jet topology yields a 20% increase in the correlator strength relative to isotropic events. Given that the production of high p_T particles and jets is known to be quenched in mid to central A–A collisions, one concludes that the observed deviation from $\langle dN_{\text{ch}}/d\eta \rangle^{-1/2}$ is likely not associated with a change in jet production but originates from other sources. A prime candidate for such a source is the large transverse radial flow arising in mid to central A–A collisions [59, 60].

Acknowledgements

The ALICE Collaboration would like to thank all its engineers and technicians for their invaluable contributions to the construction of the experiment and the CERN accelerator teams for the outstanding performance of the LHC complex. The ALICE Collaboration gratefully acknowledges the resources and support provided by all Grid centres and the Worldwide LHC Computing Grid (WLCG) collaboration. The ALICE Collaboration acknowledges the following funding agencies for their support in building and running the ALICE detector: A. I. Alikhanyan National Science Laboratory (Yerevan Physics Institute) Foundation (ANSL), State Committee of Science and World Federation of Scientists (WFS), Armenia; Austrian Academy of Sciences, Austrian Science Fund (FWF): [M 2467-N36] and Nationalstiftung für Forschung, Technologie und Entwicklung, Austria; Ministry of Communications and High Technologies, National Nuclear Research Center, Azerbaijan; Conselho Nacional de Desenvolvimento Científico e Tecnológico (CNPq), Financiadora de Estudos e Projetos (Finep), Fundação de Amparo à Pesquisa do Estado de São Paulo (FAPESP) and Universidade Federal do Rio Grande do Sul (UFRGS), Brazil; Bulgarian Ministry of Education and Science, within the National Roadmap for Research Infrastructures 2020-2027 (object CERN), Bulgaria; Ministry of Education of China (MOEC) , Ministry of Science & Technology of China (MSTC) and National Natural Science Foundation of China (NSFC), China; Ministry of Science and Education and Croatian Science Foundation, Croatia; Centro de Aplicaciones Tecnológicas y Desarrollo Nuclear (CEADEN), Cubaenergía, Cuba; Ministry of Education, Youth and Sports of the Czech Republic, Czech Republic; The Danish Council for Independent Research | Natural Sciences, the VILLUM FONDEN and Danish National Research Foundation (DNRF), Denmark; Helsinki Institute of Physics (HIP), Finland; Commissariat à l’Energie Atomique (CEA) and Institut National de Physique Nucléaire et de Physique des Particules (IN2P3) and Centre National de la Recherche Scientifique (CNRS), France; Bundesministerium für Bildung und Forschung (BMBF) and GSI Helmholtzzentrum für Schwerionenforschung GmbH, Germany; General Secretariat for Research

and Technology, Ministry of Education, Research and Religions, Greece; National Research, Development and Innovation Office, Hungary; Department of Atomic Energy Government of India (DAE), Department of Science and Technology, Government of India (DST), University Grants Commission, Government of India (UGC) and Council of Scientific and Industrial Research (CSIR), India; National Research and Innovation Agency - BRIN, Indonesia; Istituto Nazionale di Fisica Nucleare (INFN), Italy; Japanese Ministry of Education, Culture, Sports, Science and Technology (MEXT) and Japan Society for the Promotion of Science (JSPS) KAKENHI, Japan; Consejo Nacional de Ciencia (CONACYT) y Tecnología, through Fondo de Cooperación Internacional en Ciencia y Tecnología (FONCICYT) and Dirección General de Asuntos del Personal Académico (DGAPA), Mexico; Nederlandse Organisatie voor Wetenschappelijk Onderzoek (NWO), Netherlands; The Research Council of Norway, Norway; Pontificia Universidad Católica del Perú, Peru; Ministry of Science and Higher Education, National Science Centre and WUT ID-UB, Poland; Korea Institute of Science and Technology Information and National Research Foundation of Korea (NRF), Republic of Korea; Ministry of Education and Scientific Research, Institute of Atomic Physics, Ministry of Research and Innovation and Institute of Atomic Physics and Universitatea Națională de Știință și Tehnologie Politehnica București, Romania; Ministry of Education, Science, Research and Sport of the Slovak Republic, Slovakia; National Research Foundation of South Africa, South Africa; Swedish Research Council (VR) and Knut & Alice Wallenberg Foundation (KAW), Sweden; European Organization for Nuclear Research, Switzerland; Suranaree University of Technology (SUT), National Science and Technology Development Agency (NSTDA) and National Science, Research and Innovation Fund (NSRF via PMU-B B05F650021), Thailand; Turkish Energy, Nuclear and Mineral Research Agency (TENMAK), Turkey; National Academy of Sciences of Ukraine, Ukraine; Science and Technology Facilities Council (STFC), United Kingdom; National Science Foundation of the United States of America (NSF) and United States Department of Energy, Office of Nuclear Physics (DOE NP), United States of America. In addition, individual groups or members have received support from: Czech Science Foundation (grant no. 23-07499S), Czech Republic; FORTE project, reg. no. CZ.02.01.01/00/22_008/0004632, Czech Republic, co-funded by the European Union, Czech Republic; European Research Council (grant no. 950692), European Union; ICSC - Centro Nazionale di Ricerca in High Performance Computing, Big Data and Quantum Computing, European Union - NextGenerationEU; Academy of Finland (Center of Excellence in Quark Matter) (grant nos. 346327, 346328), Finland; Deutsche Forschungsgemeinschaft (DFG, German Research Foundation) “Neutrinos and Dark Matter in Astro- and Particle Physics” (grant no. SFB 1258), Germany.

References

- [1] S. Jeon and V. Koch, “Event by event fluctuations”, arXiv:hep-ph/0304012.
- [2] H. Heiselberg, “Event-by-event physics in relativistic heavy ion collisions”, *Phys. Rept.* **351** (2001) 161–194, arXiv:nucl-th/0003046.
- [3] E. V. Shuryak, “Event per event analysis of heavy ion collisions and thermodynamical fluctuations”, *Phys. Lett. B* **423** (1998) 9–14, arXiv:hep-ph/9704456.
- [4] M. A. Stephanov, K. Rajagopal, and E. V. Shuryak, “Signatures of the tricritical point in QCD”, *Phys. Rev. Lett.* **81** (1998) 4816–4819, arXiv:hep-ph/9806219.
- [5] M. A. Stephanov, K. Rajagopal, and E. V. Shuryak, “Event-by-event fluctuations in heavy ion collisions and the QCD critical point”, *Phys. Rev. D* **60** (1999) 114028, arXiv:hep-ph/9903292.
- [6] A. Dumitru and R. D. Pisarski, “Event-by-event fluctuations from decay of a Polyakov loop condensate”, *Phys. Lett. B* **504** (2001) 282–290, arXiv:hep-ph/0010083.
- [7] Z. Fodor and S. D. Katz, “Critical point of QCD at finite T and μ , lattice results for physical quark masses”, *JHEP* **04** (2004) 050, arXiv:hep-lat/0402006.

- [8] **ALICE** Collaboration, S. Acharya *et al.*, “The ALICE experiment: a journey through QCD”, *Eur. Phys. J. C* **84** (2024) 813, arXiv:2211.04384 [nucl-ex].
- [9] L. Stodolsky, “Temperature fluctuations in multiparticle production”, *Phys. Rev. Lett.* **75** (1995) 1044–1045.
- [10] S. Basu, S. Chatterjee, R. Chatterjee, T. K. Nayak, and B. K. Nandi, “Specific Heat of Matter Formed in Relativistic Nuclear Collisions”, *Phys. Rev. C* **94** (2016) 044901, arXiv:1601.05631 [nucl-ex].
- [11] **NA49** Collaboration, H. Appelshäuser *et al.*, “Event-by-event fluctuations of average transverse momentum in central Pb + Pb collisions at 158-GeV per nucleon”, *Phys. Lett. B* **459** (1999) 679–686, arXiv:hep-ex/9904014.
- [12] **CERES** Collaboration, D. Adamova *et al.*, “Event by event fluctuations of the mean transverse momentum in 40, 80 and 158 A GeV / c Pb - Au collisions”, *Nucl. Phys. A* **727** (2003) 97–119, arXiv:nucl-ex/0305002.
- [13] **NA49** Collaboration, T. Anticic *et al.*, “Energy dependence of transverse momentum fluctuations in Pb+Pb collisions at the CERN Super Proton Synchrotron (SPS) at 20A to 158A GeV”, *Phys. Rev. C* **79** (2009) 044904, arXiv:0810.5580 [nucl-ex].
- [14] G. Nijs and W. van der Schee, “Predictions and postdictions for relativistic lead and oxygen collisions with the computational simulation code Trajectum”, *Phys. Rev. C* **106** (2022) 044903, arXiv:2110.13153 [nucl-th].
- [15] **STAR** Collaboration, J. Adams *et al.*, “The Energy dependence of p_T angular correlations inferred from mean- p_T fluctuation scale dependence in heavy ion collisions at the SPS and RHIC”, *J. Phys. G* **34** (2007) 451–466, arXiv:nucl-ex/0605021.
- [16] **STAR** Collaboration, J. Adams *et al.*, “Transverse-momentum p_T correlations on (η, ϕ) from mean- p_T fluctuations in Au-Au collisions at $\sqrt{(s_{NN})} = 200$ GeV”, *J. Phys. G* **32** (2006) L37–L48, arXiv:nucl-ex/0509030.
- [17] **STAR** Collaboration, J. Adams *et al.*, “Incident energy dependence of p_T correlations at RHIC”, *Phys. Rev. C* **72** (2005) 044902, arXiv:nucl-ex/0504031.
- [18] **STAR** Collaboration, J. Adams *et al.*, “Event by event $\langle p_T \rangle$ fluctuations in Au - Au collisions at $\sqrt{(s_{NN})} = 130$ GeV”, *Phys. Rev. C* **71** (2005) 064906, arXiv:nucl-ex/0308033.
- [19] **STAR** Collaboration, J. Adam *et al.*, “Collision-energy dependence of p_T correlations in Au + Au collisions at energies available at the BNL Relativistic Heavy Ion Collider”, *Phys. Rev. C* **99** (2019) 044918, arXiv:1901.00837 [nucl-ex].
- [20] **PHENIX** Collaboration, S. S. Adler *et al.*, “Measurement of nonrandom event by event fluctuations of average transverse momentum in $\sqrt{(s_{NN})} = 200$ GeV Au+Au and p+p collisions”, *Phys. Rev. Lett.* **93** (2004) 092301, arXiv:nucl-ex/0310005.
- [21] **PHENIX** Collaboration, K. Adcox *et al.*, “Event-by-event fluctuations in mean p_T and mean e_T in $\sqrt{(s_{NN})} = 130$ GeV Au+Au collisions”, *Phys. Rev. C* **66** (2002) 024901, arXiv:nucl-ex/0203015.
- [22] **ALICE** Collaboration, B. B. Abelev *et al.*, “Event-by-event mean p_T fluctuations in pp and Pb-Pb collisions at the LHC”, *Eur. Phys. J. C* **74** (2014) 3077, arXiv:1407.5530 [nucl-ex].

- [23] C. Pruneau, S. Gavin, and S. Voloshin, “Methods for the study of particle production fluctuations”, *Phys. Rev. C* **66** (2002) 044904, arXiv:nucl-ex/0204011.
- [24] M. Sharma and C. A. Pruneau, “Methods for the Study of Transverse Momentum Differential Correlations”, *Phys. Rev. C* **79** (2009) 024905, arXiv:0810.0716 [nucl-ex].
- [25] ALICE Collaboration, S. Acharya *et al.*, “Skewness and kurtosis of mean transverse momentum fluctuations at the LHC energies”, *Phys. Lett. B* **850** (2024) 138541, arXiv:2308.16217 [nucl-ex].
- [26] S. A. Voloshin, “Transverse radial expansion in nuclear collisions and two particle correlations”, *Phys. Lett. B* **632** (2006) 490–494, arXiv:nucl-th/0312065.
- [27] S. Gavin, “Traces of thermalization from transverse momentum fluctuations in nuclear collisions”, *Phys. Rev. Lett.* **92** (2004) 162301, arXiv:nucl-th/0308067.
- [28] E. G. Ferreiro, F. del Moral, and C. Pajares, “Transverse momentum fluctuations and percolation of strings”, *Phys. Rev. C* **69** (2004) 034901, arXiv:hep-ph/0303137.
- [29] S. Gavin and G. Moschelli, “Fluctuation Probes of Early-Time Correlations in Nuclear Collisions”, *Phys. Rev. C* **85** (2012) 014905, arXiv:1107.3317 [nucl-th].
- [30] S. Gavin and G. Moschelli, “Flow Fluctuations from Early-Time Correlations in Nuclear Collisions”, *Phys. Rev. C* **86** (2012) 034902, arXiv:1205.1218 [nucl-th].
- [31] B. Alver and G. Roland, “Collision geometry fluctuations and triangular flow in heavy-ion collisions”, *Phys. Rev. C* **81** (2010) 054905, arXiv:1003.0194 [nucl-th]. [Erratum: Phys. Rev. C 82, 039903 (2010)].
- [32] ALICE Collaboration, S. Acharya *et al.*, “Charged-particle production as a function of multiplicity and transverse spherocity in pp collisions at $\sqrt{s} = 5.02$ and 13 TeV”, *Eur. Phys. J. C* **79** (2019) 857, arXiv:1905.07208 [nucl-ex].
- [33] A. Banfi, G. P. Salam, and G. Zanderighi, “Phenomenology of event shapes at hadron colliders”, *JHEP* **06** (2010) 038, arXiv:1001.4082 [hep-ph].
- [34] A. Ortiz, “Experimental results on event shapes at hadron colliders”, *Adv. Ser. Direct. High Energy Phys.* **29** (2018) 343–357, arXiv:1705.02056 [hep-ex].
- [35] S. A. Voloshin, V. Koch, and H. G. Ritter, “Event-by-event fluctuations in collective quantities”, *Phys. Rev. C* **60** (1999) 024901, arXiv:nucl-th/9903060.
- [36] S. A. Voloshin, “Mean p_T fluctuations from two particle and four particle correlations”, arXiv:nucl-th/0206052.
- [37] G. Giacalone, F. G. Gardim, J. Noronha-Hostler, and J.-Y. Ollitrault, “Skewness of mean transverse momentum fluctuations in heavy-ion collisions”, *Phys. Rev. C* **103** (2021) 024910, arXiv:2004.09799 [nucl-th].
- [38] ALICE Collaboration, B. B. Abelev *et al.*, “Multiplicity dependence of the average transverse momentum in pp, p–Pb, and Pb–Pb collisions at the LHC”, *Phys. Lett. B* **727** (2013) 371–380, arXiv:1307.1094 [nucl-ex].
- [39] ALICE Collaboration, S. Acharya *et al.*, “Light-flavor particle production in high-multiplicity pp collisions at $\sqrt{s}=13$ TeV as a function of transverse spherocity”, *JHEP* **05** (2024) 184, arXiv:2310.10236 [hep-ex].

- [40] ALICE Collaboration, K. Aamodt *et al.*, “The ALICE experiment at the CERN LHC”, *JINST* **3** (2008) S08002.
- [41] ALICE Collaboration, B. B. Abelev *et al.*, “Performance of the ALICE Experiment at the CERN LHC”, *Int.J.Mod.Phys. A* **29** (2014) 1430044, arXiv:1402.4476 [nucl-ex].
- [42] ALICE Collaboration, J. Adam *et al.*, “Centrality Dependence of the Charged-Particle Multiplicity Density at Midrapidity in Pb–Pb Collisions at $\sqrt{s_{\text{NN}}} = 5.02$ TeV”, *Phys. Rev. Lett.* **116** (2016) 222302, arXiv:1512.06104 [nucl-ex].
- [43] ALICE Collaboration, S. Acharya *et al.*, “Centrality and pseudorapidity dependence of the charged-particle multiplicity density in Xe–Xe collisions at $\sqrt{s_{\text{NN}}} = 5.44$ TeV”, *Phys. Lett. B* **790** (2019) 35–48, arXiv:1805.04432 [nucl-ex].
- [44] ALICE Collaboration, “The ALICE definition of primary particles”, *ALICE-PUBLIC-2017-005* (2017). <https://cds.cern.ch/record/2270008>.
- [45] ALICE Collaboration, S. Acharya *et al.*, “Transverse momentum spectra and nuclear modification factors of charged particles in pp, p–Pb and Pb–Pb collisions at the LHC”, *JHEP* **11** (2018) 013, arXiv:1802.09145 [nucl-ex].
- [46] R. Brun *et al.*, *GEANT: Detector Description and Simulation Tool; Oct 1994*. CERN Program Library. CERN, Geneva, 1993. <https://cds.cern.ch/record/1082634>. Long Writeup W5013.
- [47] X.-N. Wang and M. Gyulassy, “HIJING: A Monte Carlo model for multiple jet production in pp, pA and AA collisions”, *Phys. Rev. D* **44** (1991) 3501–3516.
- [48] P. Skands, S. Carrazza, and J. Rojo, “Tuning PYTHIA 8.1: the Monash 2013 Tune”, *Eur. Phys. J. C* **74** (2014) 3024, arXiv:1404.5630 [hep-ph].
- [49] Z.-W. Lin, C. M. Ko, B.-A. Li, B. Zhang, and S. Pal, “A Multi-phase transport model for relativistic heavy ion collisions”, *Phys. Rev. C* **72** (2005) 064901, arXiv:nucl-th/0411110.
- [50] K. Werner, B. Guiot, I. Karpenko, and T. Pierog, “Analysing radial flow features in p–Pb and p–p collisions at several TeV by studying identified particle production in EPOS3”, *Phys. Rev. C* **89** (2014) 064903, arXiv:1312.1233 [nucl-th].
- [51] D. Solanki, P. Sorensen, S. Basu, R. Raniwala, and T. K. Nayak, “Beam energy dependence of Elliptic and Triangular flow with the AMPT model”, *Phys. Lett. B* **720** (2013) 352–357, arXiv:1210.0512 [nucl-ex].
- [52] STAR Collaboration, M. M. Aggarwal *et al.*, “Higher Moments of Net-proton Multiplicity Distributions at RHIC”, *Phys. Rev. Lett.* **105** (2010) 022302, arXiv:1004.4959 [nucl-ex].
- [53] P. Z. Skands, “Tuning Monte Carlo Generators: The Perugia Tunes”, *Phys. Rev. D* **82** (2010) 074018, arXiv:1005.3457 [hep-ph].
- [54] T. Pierog, I. Karpenko, J. M. Katzy, E. Yatsenko, and K. Werner, “EPOS LHC: Test of collective hadronization with data measured at the CERN Large Hadron Collider”, *Phys. Rev. C* **92** (2015) 034906, arXiv:1306.0121 [hep-ph].
- [55] ALICE Collaboration, S. Acharya *et al.*, “Longitudinal and azimuthal evolution of two-particle transverse momentum correlations in Pb–Pb collisions at $\sqrt{s_{\text{NN}}} = 2.76$ TeV”, *Phys. Lett. B* **804** (2020) 135375, arXiv:1910.14393 [nucl-ex].

- [56] ATLAS Collaboration, G. Aad *et al.*, “Measurement of flow harmonics correlations with mean transverse momentum in lead-lead and proton-lead collisions at $\sqrt{s_{NN}} = 5.02$ TeV with the ATLAS detector”, *Eur. Phys. J. C* **79** (2019) 985, arXiv:1907.05176 [nucl-ex].
- [57] ALICE Collaboration, K. Aamodt *et al.*, “Higher harmonic anisotropic flow measurements of charged particles in Pb-Pb collisions at $\sqrt{s_{NN}}=2.76$ TeV”, *Phys. Rev. Lett.* **107** (2011) 032301, arXiv:1105.3865 [nucl-ex].
- [58] ALICE Collaboration, J. Adam *et al.*, “Flow dominance and factorization of transverse momentum correlations in Pb–Pb collisions at the LHC”, *Phys. Rev. Lett.* **118** (2017) 162302, arXiv:1702.02665 [nucl-ex].
- [59] ALICE Collaboration, B. Abelev *et al.*, “Centrality dependence of π , K, p production in Pb–Pb collisions at $\sqrt{s_{NN}} = 2.76$ TeV”, *Phys. Rev. C* **88** (2013) 044910, arXiv:1303.0737 [hep-ex].
- [60] I. Melo and B. Tomášik, “Blast wave fits with resonances to p_T spectra from nuclear collisions at the LHC”, *J. Phys. Conf. Ser.* **668** (2016) 012070, arXiv:1509.05383 [nucl-th].
- [61] S. A. Voloshin, “Heavy ion collisions: Correlations and fluctuations in particle production”, *J. Phys. Conf. Ser.* **50** (2006) 111–118, arXiv:nucl-ex/0505003.
- [62] T. Sjostrand, S. Mrenna, and P. Z. Skands, “PYTHIA 6.4 Physics and Manual”, *JHEP* **05** (2006) 026, arXiv:hep-ph/0603175.
- [63] P. Huovinen, P. F. Kolb, U. W. Heinz, P. V. Ruuskanen, and S. A. Voloshin, “Radial and elliptic flow at RHIC: Further predictions”, *Phys. Lett. B* **503** (2001) 58–64, arXiv:hep-ph/0101136.

A The ALICE Collaboration

- S. Acharya ¹²⁶, A. Agarwal¹³⁴, G. Aglieri Rinella ³², L. Aglietta ²⁴, M. Agnello ²⁹, N. Agrawal ²⁵, Z. Ahammed ¹³⁴, S. Ahmad ¹⁵, S.U. Ahn ⁷¹, I. Ahuja ³⁶, A. Akindinov ¹⁴⁰, V. Akishina³⁸, M. Al-Turany ⁹⁶, D. Aleksandrov ¹⁴⁰, B. Alessandro ⁵⁶, H.M. Alfanda ⁶, R. Alfaro Molina ⁶⁷, B. Ali ¹⁵, A. Alici ²⁵, N. Alizadehvandchali ¹¹⁵, A. Alkin ¹⁰³, J. Alme ²⁰, G. Alocco ^{24,52}, T. Alt ⁶⁴, A.R. Altamura ⁵⁰, I. Altsybeev ⁹⁴, J.R. Alvarado ⁴⁴, C.O.R. Alvarez ⁴⁴, M.N. Anaam ⁶, C. Andrei ⁴⁵, N. Andreou ¹¹⁴, A. Andronic ¹²⁵, E. Andronov ¹⁴⁰, V. Anguelov ⁹³, F. Antinori ⁵⁴, P. Antonioli ⁵¹, N. Apadula ⁷³, L. Aphecetche ¹⁰², H. Appelshäuser ⁶⁴, C. Arata ⁷², S. Arcelli ²⁵, R. Arnaldi ⁵⁶, J.G.M.C.A. Arneiro ¹⁰⁹, I.C. Arsene ¹⁹, M. Arslanbekov ¹³⁷, A. Augustinus ³², R. Averbeck ⁹⁶, D. Averyanov ¹⁴⁰, M.D. Azmi ¹⁵, H. Baba ¹²³, A. Badalà ⁵³, J. Bae ¹⁰³, Y. Bae ¹⁰³, Y.W. Baek ⁴⁰, X. Bai ¹¹⁹, R. Bailhache ⁶⁴, Y. Bailung ⁴⁸, R. Bala ⁹⁰, A. Balbino ²⁹, A. Baldissari ¹²⁹, B. Balis ², Z. Banoo ⁹⁰, V. Barbasova³⁶, F. Barile ³¹, L. Barioglio ⁵⁶, M. Barlou ⁷⁷, B. Barman⁴¹, G.G. Barnaföldi ⁴⁶, L.S. Barnby ¹¹⁴, E. Barreau ¹⁰², V. Barret ¹²⁶, L. Barreto ¹⁰⁹, C. Bartels ¹¹⁸, K. Barth ³², E. Bartsch ⁶⁴, N. Bastid ¹²⁶, S. Basu ⁷⁴, G. Batigne ¹⁰², D. Battistini ⁹⁴, B. Batyunya ¹⁴¹, D. Bauri⁴⁷, J.L. Bazo Alba ¹⁰⁰, I.G. Bearden ⁸², C. Beattie ¹³⁷, P. Becht ⁹⁶, D. Behera ⁴⁸, I. Belikov ¹²⁸, A.D.C. Bell Hechavarria ¹²⁵, F. Bellini ²⁵, R. Bellwied ¹¹⁵, S. Belokurova ¹⁴⁰, L.G.E. Beltran ¹⁰⁸, Y.A.V. Beltran ⁴⁴, G. Bencedi ⁴⁶, A. Bensaoula ¹¹⁵, S. Beole ²⁴, Y. Berdnikov ¹⁴⁰, A. Berdnikova ⁹³, L. Bergmann ⁹³, M.G. Besoiu ⁶³, L. Betev ³², P.P. Bhaduri ¹³⁴, A. Bhasin ⁹⁰, B. Bhattacharjee ⁴¹, L. Bianchi ²⁴, J. Bielčík ³⁴, J. Bielčíková ⁸⁵, A.P. Bigot ¹²⁸, A. Bilandzic ⁹⁴, G. Biro ⁴⁶, S. Biswas ⁴, N. Bize ¹⁰², J.T. Blair ¹⁰⁷, D. Blau ¹⁴⁰, M.B. Blidaru ⁹⁶, N. Bluhme³⁸, C. Blume ⁶⁴, F. Bock ⁸⁶, T. Bodova ²⁰, J. Bok ¹⁶, L. Boldizsár ⁴⁶, M. Bombara ³⁶, P.M. Bond ³², G. Bonomi ^{133,55}, H. Borel ¹²⁹, A. Borissov ¹⁴⁰, A.G. Borquez Carcamo ⁹³, E. Botta ²⁴, Y.E.M. Bouziani ⁶⁴, L. Bratrud ⁶⁴, P. Braun-Munzinger ⁹⁶, M. Bregant ¹⁰⁹, M. Broz ³⁴, G.E. Bruno ^{95,31}, V.D. Buchakchiev ³⁵, M.D. Buckland ⁸⁴, D. Budnikov ¹⁴⁰, H. Buesching ⁶⁴, S. Bufalino ²⁹, P. Buhler ¹⁰¹, N. Burmasov ¹⁴⁰, Z. Buthelezi ^{68,122}, A. Bylinkin ²⁰, S.A. Bysiak¹⁰⁶, J.C. Cabanillas Noris ¹⁰⁸, M.F.T. Cabrera¹¹⁵, H. Caines ¹³⁷, A. Caliva ²⁸, E. Calvo Villar ¹⁰⁰, J.M.M. Camacho ¹⁰⁸, P. Camerini ²³, F.D.M. Canedo ¹⁰⁹, S.L. Cantway ¹³⁷, M. Carabas ¹¹², A.A. Carballo ³², F. Carnesecchi ³², R. Caron ¹²⁷, L.A.D. Carvalho ¹⁰⁹, J. Castillo Castellanos ¹²⁹, M. Castoldi ³², F. Catalano ³², S. Cattaruzzi ²³, R. Cerri ²⁴, I. Chakaberia ⁷³, P. Chakraborty ¹³⁵, S. Chandra ¹³⁴, S. Chapelard ³², M. Chartier ¹¹⁸, S. Chattopadhyay¹³⁴, M. Chen³⁹, T. Cheng ⁶, C. Cheshkov ¹²⁷, D. Chiappara ²⁷, V. Chibante Barroso ³², D.D. Chinellato ¹⁰¹, E.S. Chizzali ^{II,94}, J. Cho ⁵⁸, S. Cho ⁵⁸, P. Chochula ³², Z.A. Chochulska ¹³⁵, D. Choudhury⁴¹, S. Choudhury⁹⁸, P. Christakoglou ⁸³, C.H. Christensen ⁸², P. Christiansen ⁷⁴, T. Chujo ¹²⁴, M. Ciacco ²⁹, C. Cicalo ⁵², F. Cindolo ⁵¹, M.R. Ciupek⁹⁶, G. Clai^{III,51}, F. Colamarria ⁵⁰, J.S. Colburn⁹⁹, D. Colella ³¹, A. Colelli³¹, M. Colocci ²⁵, M. Concas ³², G. Conesa Balbastre ⁷², Z. Conesa del Valle ¹³⁰, G. Contin ²³, J.G. Contreras ³⁴, M.L. Coquet ¹⁰², P. Cortese ^{132,56}, M.R. Cosentino ¹¹¹, F. Costa ³², S. Costanza ^{21,55}, C. Cot ¹³⁰, P. Crochet ¹²⁶, M.M. Czarnynoga¹³⁵, A. Dainese ⁵⁴, G. Dange³⁸, M.C. Danisch ⁹³, A. Danu ⁶³, P. Das ^{32,79}, S. Das ⁴, A.R. Dash ¹²⁵, S. Dash ⁴⁷, A. De Caro ²⁸, G. de Cataldo ⁵⁰, J. de Cuveland³⁸, A. De Falco ²², D. De Gruttola ²⁸, N. De Marco ⁵⁶, C. De Martin ²³, S. De Pasquale ²⁸, R. Deb ¹³³, R. Del Grande ⁹⁴, L. Dello Stritto ³², W. Deng ⁶, K.C. Devereaux¹⁸, G.G.A. de Souza¹⁰⁹, P. Dhankher ¹⁸, D. Di Bari ³¹, A. Di Mauro ³², B. Di Ruzza ¹³¹, B. Diab ¹²⁹, R.A. Diaz ^{141,7}, Y. Ding ⁶, J. Ditzel ⁶⁴, R. Divià ³², Ø. Djupsland²⁰, U. Dmitrieva ¹⁴⁰, A. Dobrin ⁶³, B. Dönigus ⁶⁴, J.M. Dubinski ¹³⁵, A. Dubla ⁹⁶, P. Dupieux ¹²⁶, N. Dzalaiova¹³, T.M. Eder ¹²⁵, R.J. Ehlers ⁷³, F. Eisenhut ⁶⁴, R. Ejima ⁹¹, D. Elia ⁵⁰, B. Erazmus ¹⁰², F. Ercolelli ²⁵, B. Espagnon ¹³⁰, G. Eulisse ³², D. Evans ⁹⁹, S. Evdokimov ¹⁴⁰, L. Fabbietti ⁹⁴, M. Faggin ²³, J. Faivre ⁷², F. Fan ⁶, W. Fan ⁷³, A. Fantoni ⁴⁹, M. Fasel ⁸⁶, G. Feofilov ¹⁴⁰, A. Fernández Téllez ⁴⁴, L. Ferrandi ¹⁰⁹, M.B. Ferrer ³², A. Ferrero ¹²⁹, C. Ferrero ^{IV,56}, A. Ferretti ²⁴, V.J.G. Feuillard ⁹³, V. Filova ³⁴, D. Finogeev ¹⁴⁰, F.M. Fionda ⁵², E. Flatland³², F. Flor ^{137,115}, A.N. Flores ¹⁰⁷, S. Foertsch ⁶⁸, I. Fokin ⁹³, S. Fokin ¹⁴⁰, U. Follo ^{IV,56}, E. Fragiocomo ⁵⁷, E. Frajna ⁴⁶, U. Fuchs ³², N. Funicello ²⁸, C. Furget ⁷², A. Furs ¹⁴⁰, T. Fusayasu ⁹⁷, J.J. Gaardhøje ⁸², M. Gagliardi ²⁴, A.M. Gago ¹⁰⁰, T. Gahlaut⁴⁷, C.D. Galvan ¹⁰⁸, S. Gami⁷⁹, D.R. Gangadharan ¹¹⁵, P. Ganoti ⁷⁷, C. Garabatos ⁹⁶, J.M. Garcia ⁴⁴, T. García Chávez ⁴⁴, E. Garcia-Solis ⁹, C. Gargiulo ³², P. Gasik ⁹⁶, H.M. Gaur³⁸, A. Gautam ¹¹⁷, M.B. Gay Ducati ⁶⁶, M. Germain ¹⁰², R.A. Gernhaeuser⁹⁴, C. Ghosh¹³⁴, M. Giacalone ⁵¹, G. Gioachin ²⁹, S.K. Giri¹³⁴, P. Giubellino ^{96,56}, P. Giubilato ²⁷, A.M.C. Glaenzer ¹²⁹, P. Glässel ⁹³, E. Glimos ¹²¹, D.J.Q. Goh⁷⁵, V. Gonzalez ¹³⁶, P. Gordeev ¹⁴⁰, M. Gorgon ², K. Goswami ⁴⁸, S. Gotovac ³³, V. Grabski ⁶⁷, L.K. Graczykowski ¹³⁵, E. Grecka ⁸⁵, A. Grelli ⁵⁹, C. Grigoras ³², V. Grigoriev ¹⁴⁰, S. Grigoryan ^{141,1},

- F. Grossa ³², J.F. Grosse-Oetringhaus ³², R. Grossos ⁹⁶, D. Grund ³⁴, N.A. Grunwald ⁹³,
 G.G. Guardiano ¹¹⁰, R. Guernane ⁷², M. Guilbaud ¹⁰², K. Gulbrandsen ⁸², J.J.W.K. Gumprecht ¹⁰¹,
 T. Gündem ⁶⁴, T. Gunji ¹²³, W. Guo ⁶, A. Gupta ⁹⁰, R. Gupta ⁹⁰, R. Gupta ⁴⁸, K. Gwizdziel ¹³⁵,
 L. Gyulai ⁴⁶, C. Hadjidakis ¹³⁰, F.U. Haider ⁹⁰, S. Haidlova ³⁴, M. Haldar ⁴, H. Hamagaki ⁷⁵,
 Y. Han ¹³⁹, B.G. Hanley ¹³⁶, R. Hannigan ¹⁰⁷, J. Hansen ⁷⁴, M.R. Haque ⁹⁶, J.W. Harris ¹³⁷,
 A. Harton ⁹, M.V. Hartung ⁶⁴, H. Hassan ¹¹⁶, D. Hatzifotiadou ⁵¹, P. Hauer ⁴², L.B. Havener ¹³⁷,
 E. Hellbär ³², H. Helstrup ³⁷, M. Hemmer ⁶⁴, T. Herman ³⁴, S.G. Hernandez ¹¹⁵, G. Herrera Corral ⁸,
 S. Herrmann ¹²⁷, K.F. Hetland ³⁷, B. Heybeck ⁶⁴, H. Hillemanns ³², B. Hippolyte ¹²⁸, I.P.M. Hobus ⁸³,
 F.W. Hoffmann ⁷⁰, B. Hofman ⁵⁹, M. Horst ⁹⁴, A. Horzyk ², Y. Hou ⁶, P. Hristov ³², P. Huhn ⁶⁴,
 L.M. Huhta ¹¹⁶, T.J. Humanic ⁸⁷, A. Hutson ¹¹⁵, D. Hutter ³⁸, M.C. Hwang ¹⁸, R. Ilkaev ¹⁴⁰,
 M. Inaba ¹²⁴, G.M. Innocenti ³², M. Ippolitov ¹⁴⁰, A. Isakov ⁸³, T. Isidori ¹¹⁷, M.S. Islam ^{47,98},
 S. Iurchenko ¹⁴⁰, M. Ivanov ⁹⁶, M. Ivanov ¹³, V. Ivanov ¹⁴⁰, K.E. Iversen ⁷⁴, M. Jablonski ²,
 B. Jacak ^{18,73}, N. Jacazio ²⁵, P.M. Jacobs ⁷³, S. Jadlovská ¹⁰⁵, J. Jadlovsky ¹⁰⁵, S. Jaelani ⁸¹, C. Jahnke ¹⁰⁹,
 M.J. Jakubowska ¹³⁵, M.A. Janik ¹³⁵, T. Janson ⁷⁰, S. Ji ¹⁶, S. Jia ¹⁰, T. Jiang ¹⁰, A.A.P. Jimenez ⁶⁵,
 F. Jonas ⁷³, D.M. Jones ¹¹⁸, J.M. Jowett ^{32,96}, J. Jung ⁶⁴, M. Jung ⁶⁴, A. Junique ³², A. Jusko ⁹⁹,
 J. Kaewjai ¹⁰⁴, P. Kalinak ⁶⁰, A. Kalweit ³², A. Karasu Uysal ¹³⁸, D. Karatovic ⁸⁸, N. Karatzenis ⁹⁹,
 O. Karavichev ¹⁴⁰, T. Karavicheva ¹⁴⁰, E. Karpechev ¹⁴⁰, M.J. Karwowska ¹³⁵, U. Kebschull ⁷⁰,
 M. Keil ³², B. Ketzer ⁴², J. Keul ⁶⁴, S.S. Khade ⁴⁸, A.M. Khan ¹¹⁹, S. Khan ¹⁵, A. Khanzadeev ¹⁴⁰,
 Y. Kharlov ¹⁴⁰, A. Khatun ¹¹⁷, A. Khuntia ³⁴, Z. Khuranova ⁶⁴, B. Kileng ³⁷, B. Kim ¹⁰³, C. Kim ¹⁶,
 D.J. Kim ¹¹⁶, D. Kim ¹⁰³, E.J. Kim ⁶⁹, J. Kim ¹³⁹, J. Kim ⁵⁸, J. Kim ^{32,69}, M. Kim ¹⁸, S. Kim ¹⁷,
 T. Kim ¹³⁹, K. Kimura ⁹¹, A. Kirkova ³⁵, S. Kirsch ⁶⁴, I. Kisiel ³⁸, S. Kiselev ¹⁴⁰, A. Kisiel ¹³⁵,
 J.L. Klay ⁵, J. Klein ³², S. Klein ⁷³, C. Klein-Bösing ¹²⁵, M. Kleiner ⁶⁴, T. Klemenz ⁹⁴, A. Kluge ³²,
 C. Kobdaj ¹⁰⁴, R. Kohara ¹²³, T. Kollegger ⁹⁶, A. Kondratyev ¹⁴¹, N. Kondratyeva ¹⁴⁰, J. Konig ⁶⁴,
 S.A. Konigstorfer ⁹⁴, P.J. Konopka ³², G. Kornakov ¹³⁵, M. Korwieser ⁹⁴, S.D. Koryciak ², C. Koster ⁸³,
 A. Kotliarov ⁸⁵, N. Kovacic ⁸⁸, V. Kovalenko ¹⁴⁰, M. Kowalski ¹⁰⁶, V. Kozhuharov ³⁵, G. Kozlov ³⁸,
 I. Králik ⁶⁰, A. Kravčáková ³⁶, L. Krcal ^{32,38}, M. Krivda ^{99,60}, F. Krizek ⁸⁵, K. Krizkova Gajdosova ³²,
 C. Krug ⁶⁶, M. Krüger ⁶⁴, D.M. Krupova ³⁴, E. Kryshen ¹⁴⁰, V. Kučera ⁵⁸, C. Kuhn ¹²⁸,
 P.G. Kuijer ⁸³, T. Kumaoka ¹²⁴, D. Kumar ¹³⁴, L. Kumar ⁸⁹, N. Kumar ⁸⁹, S. Kumar ⁵⁰, S. Kundu ³²,
 P. Kurashvili ⁷⁸, A.B. Kurepin ¹⁴⁰, A. Kuryakin ¹⁴⁰, S. Kushpil ⁸⁵, V. Kuskov ¹⁴⁰, M. Kutyla ¹³⁵,
 A. Kuznetsov ¹⁴¹, M.J. Kweon ⁵⁸, Y. Kwon ¹³⁹, S.L. La Pointe ³⁸, P. La Rocca ²⁶, A. Lakrathok ¹⁰⁴,
 M. Lamanna ³², A.R. Landou ⁷², R. Langoy ¹²⁰, P. Larionov ³², E. Laudi ³², L. Lautner ⁹⁴,
 R.A.N. Laveaga ¹⁰⁸, R. Lavicka ¹⁰¹, R. Lea ^{133,55}, H. Lee ¹⁰³, I. Legrand ⁴⁵, G. Legras ¹²⁵,
 J. Lehrbach ³⁸, A.M. Lejeune ³⁴, T.M. Lelek ², R.C. Lemmon ^{1,84}, I. León Monzón ¹⁰⁸, M.M. Lesch ⁹⁴,
 P. Lévai ⁴⁶, M. Li ⁶, P. Li ¹⁰, X. Li ¹⁰, B.E. Liang-gilman ¹⁸, J. Lien ¹²⁰, R. Lietava ⁹⁹, I. Likmeta ¹¹⁵,
 B. Lim ²⁴, H. Lim ¹⁶, S.H. Lim ¹⁶, V. Lindenstruth ³⁸, C. Lippmann ⁹⁶, D. Liskova ¹⁰⁵, D.H. Liu ⁶,
 J. Liu ¹¹⁸, G.S.S. Liveraro ¹¹⁰, I.M. Lofnes ²⁰, C. Loizides ⁸⁶, S. Lokos ¹⁰⁶, J. Lömkér ⁵⁹,
 X. Lopez ¹²⁶, E. López Torres ⁷, C. Lotteau ¹²⁷, P. Lu ^{96,119}, Z. Lu ¹⁰, F.V. Lugo ⁶⁷, J.R. Luhder ¹²⁵,
 G. Luparello ⁵⁷, Y.G. Ma ³⁹, M. Mager ³², A. Maire ¹²⁸, E.M. Majerz ², M.V. Makarieva ³⁵,
 M. Malaev ¹⁴⁰, G. Malfattore ²⁵, N.M. Malik ⁹⁰, S.K. Malik ⁹⁰, D. Mallick ¹³⁰, N. Mallick ^{116,48},
 G. Mandaglio ^{30,53}, S.K. Mandal ⁷⁸, A. Manea ⁶³, V. Manko ¹⁴⁰, F. Manso ¹²⁶, V. Manzari ⁵⁰,
 Y. Mao ⁶, R.W. Marcjan ², G.V. Margagliotti ²³, A. Margotti ⁵¹, A. Marín ⁹⁶, C. Markert ¹⁰⁷,
 C.F.B. Marquez ³¹, P. Martinengo ³², M.I. Martínez ⁴⁴, G. Martínez García ¹⁰², M.P.P. Martins ¹⁰⁹,
 S. Masciocchi ⁹⁶, M. Masera ²⁴, A. Masoni ⁵², L. Massacrier ¹³⁰, O. Massen ⁵⁹, A. Mastroserio ^{131,50},
 S. Mattiazzo ²⁷, A. Matyja ¹⁰⁶, F. Mazzaschi ^{32,24}, M. Mazzilli ¹¹⁵, Y. Melikyan ⁴³, M. Melo ¹⁰⁹,
 A. Menchaca-Rocha ⁶⁷, J.E.M. Mendez ⁶⁵, E. Meninno ¹⁰¹, A.S. Menon ¹¹⁵, M.W. Menzel ^{32,93},
 M. Meres ¹³, L. Micheletti ³², D. Mihai ¹¹², D.L. Mihaylov ⁹⁴, K. Mihaylov ^{141,140}, N. Minafra ¹¹⁷,
 D. Miśkowiec ⁹⁶, A. Modak ¹³³, B. Mohanty ⁷⁹, M. Mohisin Khan ^{V,15}, M.A. Molander ⁴³,
 M.M. Mondal ⁷⁹, S. Monira ¹³⁵, C. Mordasini ¹¹⁶, D.A. Moreira De Godoy ¹²⁵, I. Morozov ¹⁴⁰,
 A. Morsch ³², T. Mrnjavac ³², V. Muccifora ⁴⁹, S. Muhuri ¹³⁴, J.D. Mulligan ⁷³, A. Mulliri ²²,
 M.G. Munhoz ¹⁰⁹, R.H. Munzer ⁶⁴, H. Murakami ¹²³, S. Murray ¹¹³, L. Musa ³², J. Musinsky ⁶⁰,
 J.W. Myrcha ¹³⁵, B. Naik ¹²², A.I. Nambrath ¹⁸, B.K. Nandi ⁴⁷, R. Nania ⁵¹, E. Nappi ⁵⁰,
 A.F. Nassirpour ¹⁷, V. Nastase ¹¹², A. Nath ⁹³, S. Nath ¹³⁴, C. Nattrass ¹²¹, T.K. Nayak ^{115,79},
 M.N. Naydenov ³⁵, A. Neagu ¹⁹, A. Negru ¹¹², E. Nekrasova ¹⁴⁰, L. Nellen ⁶⁵, R. Nepeivoda ⁷⁴, S. Nese ¹⁹,
 N. Nicassio ³¹, B.S. Nielsen ⁸², E.G. Nielsen ⁸², S. Nikolaev ¹⁴⁰, V. Nikulin ¹⁴⁰, F. Noferini ⁵¹,
 S. Noh ¹², P. Nomokonov ¹⁴¹, J. Norman ¹¹⁸, N. Novitzky ⁸⁶, P. Nowakowski ¹³⁵, A. Nyani ¹⁴⁰,
 J. Nystrand ²⁰, S. Oh ¹⁷, A. Ohlson ⁷⁴, V.A. Okorokov ¹⁴⁰, J. Oleniacz ¹³⁵, A. Onnerstad ¹¹⁶,

- C. Oppedisano ⁵⁶, A. Ortiz Velasquez ⁶⁵, J. Otwinowski ¹⁰⁶, M. Oya ⁹¹, K. Oyama ⁷⁵, S. Padhan ⁴⁷,
 D. Pagano ^{133,55}, G. Paić ⁶⁵, S. Paisano-Guzmán ⁴⁴, A. Palasciano ⁵⁰, I. Panasenko ⁷⁴, S. Panebianco ¹²⁹,
 C. Pantouvakis ²⁷, H. Park ¹²⁴, J. Park ¹²⁴, S. Park ¹⁰³, J.E. Parkkila ³², Y. Patley ⁴⁷, R.N. Patra ⁵⁰,
 B. Paul ¹³⁴, H. Pei ⁶, T. Peitzmann ⁵⁹, X. Peng ¹¹, M. Pennisi ²⁴, S. Perciballi ²⁴, D. Peresunko ¹⁴⁰,
 G.M. Perez ⁷, Y. Pestov ¹⁴⁰, M.T. Petersen ⁸², V. Petrov ¹⁴⁰, M. Petrovici ⁴⁵, S. Piano ⁵⁷, M. Pikna ¹³,
 P. Pillot ¹⁰², O. Pinazza ^{51,32}, L. Pinsky ¹¹⁵, C. Pinto ⁹⁴, S. Pisano ⁴⁹, M. Płoskoń ⁷³, M. Planinic ⁸⁸,
 D.K. Plociennik ², M.G. Poghosyan ⁸⁶, B. Polichtchouk ¹⁴⁰, S. Politano ²⁹, N. Poljak ⁸⁸, A. Pop ⁴⁵,
 S. Porteboeuf-Houssais ¹²⁶, V. Pozdniakov ^{1,141}, I.Y. Pozos ⁴⁴, K.K. Pradhan ⁴⁸, S.K. Prasad ⁴,
 S. Prasad ⁴⁸, R. Preghenella ⁵¹, F. Prino ⁵⁶, C.A. Pruneau ¹³⁶, I. Pshenichnov ¹⁴⁰, M. Puccio ³²,
 S. Pucillo ²⁴, S. Qiu ⁸³, L. Quaglia ²⁴, A.M.K. Radhakrishnan ⁴⁸, S. Ragoni ¹⁴, A. Rai ¹³⁷,
 A. Rakotozafindrabe ¹²⁹, L. Ramello ^{132,56}, M. Rasa ²⁶, S.S. Räsänen ⁴³, R. Rath ⁵¹, M.P. Rauch ²⁰,
 I. Ravasenga ³², K.F. Read ^{86,121}, C. Reckziegel ¹¹¹, A.R. Redelbach ³⁸, K. Redlich ^{VI,78},
 C.A. Reetz ⁹⁶, H.D. Regules-Medel ⁴⁴, A. Rehman ²⁰, F. Reidt ³², H.A. Reme-Ness ³⁷, K. Reygers ⁹³,
 A. Riabov ¹⁴⁰, V. Riabov ¹⁴⁰, R. Ricci ²⁸, M. Richter ²⁰, A.A. Riedel ⁹⁴, W. Riegler ³²,
 A.G. Riffero ²⁴, M. Rignanese ²⁷, C. Ripoli ²⁸, C. Ristea ⁶³, M.V. Rodriguez ³², M. Rodríguez
 Cahuantzi ⁴⁴, S.A. Rodríguez Ramírez ⁴⁴, K. Røed ¹⁹, R. Rogalev ¹⁴⁰, E. Rogochaya ¹⁴¹,
 T.S. Rogoschinski ⁶⁴, D. Rohr ³², D. Röhrich ²⁰, S. Rojas Torres ³⁴, P.S. Rokita ¹³⁵, G. Romanenko ²⁵,
 F. Ronchetti ³², E.D. Rosas ⁶⁵, K. Roslon ¹³⁵, A. Rossi ⁵⁴, A. Roy ⁴⁸, S. Roy ⁴⁷, N. Rubini ^{51,25},
 J.A. Rudolph ⁸³, D. Ruggiano ¹³⁵, R. Rui ²³, P.G. Russek ², R. Russo ⁸³, A. Rustamov ⁸⁰,
 E. Ryabinkin ¹⁴⁰, Y. Ryabov ¹⁴⁰, A. Rybicki ¹⁰⁶, J. Ryu ¹⁶, W. Rzesz ¹³⁵, B. Sabiu ⁵¹, S. Sadovsky ¹⁴⁰,
 J. Saetre ²⁰, S. Saha ⁷⁹, B. Sahoo ⁴⁸, R. Sahoo ⁴⁸, S. Sahoo ⁶¹, D. Sahu ⁴⁸, P.K. Sahu ⁶¹, J. Saini ¹³⁴,
 K. Sajdakova ³⁶, S. Sakai ¹²⁴, M.P. Salvan ⁹⁶, S. Sambyal ⁹⁰, D. Samitz ¹⁰¹, I. Sanna ^{32,94},
 T.B. Saramela ¹⁰⁹, D. Sarkar ⁸², P. Sarma ⁴¹, V. Sarritzu ²², V.M. Sarti ⁹⁴, M.H.P. Sas ³², S. Sawan ⁷⁹,
 E. Scapparone ⁵¹, J. Schambach ⁸⁶, H.S. Scheid ⁶⁴, C. Schiaua ⁴⁵, R. Schicker ⁹³, F. Schlepper ⁹³,
 A. Schmah ⁹⁶, C. Schmidt ⁹⁶, M.O. Schmidt ³², M. Schmidt ⁹², N.V. Schmidt ⁸⁶, A.R. Schmier ¹²¹,
 J. Schoengarth ⁶⁴, R. Schotter ^{101,128}, A. Schröter ³⁸, J. Schukraft ³², K. Schweda ⁹⁶, G. Scioli ²⁵,
 E. Scomparin ⁵⁶, J.E. Seger ¹⁴, Y. Sekiguchi ¹²³, D. Sekihata ¹²³, M. Selina ⁸³, I. Selyuzhenkov ⁹⁶,
 S. Senyukov ¹²⁸, J.J. Seo ⁹³, D. Serebryakov ¹⁴⁰, L. Serkin ^{VII,65}, L. Šerkšnyté ⁹⁴, A. Sevcenco ⁶³,
 T.J. Shaba ⁶⁸, A. Shabetai ¹⁰², R. Shahoyan ³², A. Shangaraev ¹⁴⁰, B. Sharma ⁹⁰, D. Sharma ⁴⁷,
 H. Sharma ⁵⁴, M. Sharma ⁹⁰, S. Sharma ⁷⁵, S. Sharma ⁹⁰, U. Sharma ⁹⁰, A. Shatat ¹³⁰,
 O. Sheibani ^{136,115}, K. Shigaki ⁹¹, M. Shimomura ⁷⁶, J. Shin ¹², S. Shirinkin ¹⁴⁰, Q. Shou ³⁹, Y. Sibiriak ¹⁴⁰,
 S. Siddhanta ⁵², T. Siemiaczuk ⁷⁸, T.F. Silva ¹⁰⁹, D. Silvermyr ⁷⁴, T. Simantathammakul ¹⁰⁴,
 R. Simeonov ³⁵, B. Singh ⁹⁰, B. Singh ⁹⁴, K. Singh ⁴⁸, R. Singh ⁷⁹, R. Singh ⁹⁰, R. Singh ^{54,96},
 S. Singh ¹⁵, V.K. Singh ¹³⁴, V. Singhal ¹³⁴, T. Sinha ⁹⁸, B. Sitar ¹³, M. Sitta ^{132,56}, T.B. Skaali ¹⁹,
 G. Skorodumovs ⁹³, N. Smirnov ¹³⁷, R.J.M. Snellings ⁵⁹, E.H. Solheim ¹⁹, C. Sonnabend ^{32,96},
 J.M. Sonneveld ⁸³, F. Soramel ²⁷, A.B. Soto-hernandez ⁸⁷, R. Spijkers ⁸³, I. Sputowska ¹⁰⁶, J. Staa ⁷⁴,
 J. Stachel ⁹³, I. Stan ⁶³, P.J. Steffanic ¹²¹, T. Stellhorn ¹²⁵, S.F. Stiefelmaier ⁹³, D. Stocco ¹⁰²,
 I. Storehaug ¹⁹, N.J. Strangmann ⁶⁴, P. Stratmann ¹²⁵, S. Strazzi ²⁵, A. Sturniolo ^{30,53}, C.P. Stylianidis ⁸³,
 A.A.P. Suaide ¹⁰⁹, C. Suire ¹³⁰, A. Suiu ^{32,112}, M. Sukhanov ¹⁴⁰, M. Suljic ³², R. Sultanov ¹⁴⁰,
 V. Sumberia ⁹⁰, S. Sumowidagdo ⁸¹, L.H. Tabares ⁷, S.F. Taghavi ⁹⁴, J. Takahashi ¹¹⁰,
 G.J. Tambave ⁷⁹, S. Tang ⁶, Z. Tang ¹¹⁹, J.D. Tapia Takaki ¹¹⁷, N. Tapus ¹¹², L.A. Tarasovicova ³⁶,
 M.G. Tarzila ⁴⁵, A. Tauro ³², A. Tavira García ¹³⁰, G. Tejeda Muñoz ⁴⁴, L. Terlizzi ²⁴, C. Terrevoli ⁵⁰,
 S. Thakur ⁴, M. Thogersen ¹⁹, D. Thomas ¹⁰⁷, A. Tikhonov ¹⁴⁰, N. Tiltmann ^{32,125}, A.R. Timmins ¹¹⁵,
 M. Tkacik ¹⁰⁵, T. Tkacik ¹⁰⁵, A. Toia ⁶⁴, R. Tokumoto ⁹¹, S. Tomassini ²⁵, K. Tomohiro ⁹¹,
 N. Topilskaya ¹⁴⁰, M. Toppi ⁴⁹, V.V. Torres ¹⁰², A.G. Torres Ramos ³¹, A. Trifirò ^{30,53}, T. Triloki ⁹⁵,
 A.S. Triolo ^{32,30,53}, S. Tripathy ³², T. Tripathy ⁴⁷, S. Trogolo ²⁴, V. Trubnikov ³, W.H. Trzaska ¹¹⁶,
 T.P. Trzcinski ¹³⁵, C. Tsolanta ¹⁹, R. Tu ³⁹, A. Tumkin ¹⁴⁰, R. Turrisi ⁵⁴, T.S. Tveter ¹⁹, K. Ullaland ²⁰,
 B. Ulukutlu ⁹⁴, S. Upadhyaya ¹⁰⁶, A. Uras ¹²⁷, G.L. Usai ²², M. Vala ³⁶, N. Valle ⁵⁵, L.V.R. van
 Doremalen ⁵⁹, M. van Leeuwen ⁸³, C.A. van Veen ⁹³, R.J.G. van Weelden ⁸³, P. Vande Vyvre ³²,
 D. Varga ⁴⁶, Z. Varga ^{137,46}, P. Vargas Torres ⁶⁵, M. Vasileiou ⁷⁷, A. Vasiliev ^{I,140}, O. Vázquez Doce ⁴⁹,
 O. Vazquez Rueda ¹¹⁵, V. Vechernin ¹⁴⁰, E. Vercellin ²⁴, R. Verma ⁴⁷, R. Vértesi ⁴⁶, M. Verweij ⁵⁹,
 L. Vickovic ³³, Z. Vilakazi ¹²², O. Villalobos Baillie ⁹⁹, A. Villani ²³, A. Vinogradov ¹⁴⁰, T. Virgili ²⁸,
 M.M.O. Virta ¹¹⁶, A. Vodopyanov ¹⁴¹, B. Volkel ³², M.A. Völkli ⁹³, S.A. Voloshin ¹³⁶, G. Volpe ³¹,
 B. von Haller ³², I. Vorobyev ³², N. Vozniuk ¹⁴⁰, J. Vrláková ³⁶, J. Wan ³⁹, C. Wang ³⁹, D. Wang ³⁹,
 Y. Wang ³⁹, Y. Wang ⁶, Z. Wang ³⁹, A. Wegrzynek ³², F.T. Weiglhofer ³⁸, S.C. Wenzel ³²,
 J.P. Wessels ¹²⁵, P.K. Wiacek ², J. Wiechula ⁶⁴, J. Wikne ¹⁹, G. Wilk ⁷⁸, J. Wilkinson ⁹⁶,

G.A. Willems ¹²⁵, B. Windelband ⁹³, M. Winn ¹²⁹, J.R. Wright ¹⁰⁷, W. Wu ³⁹, Y. Wu ¹¹⁹, Z. Xiong ¹¹⁹, R. Xu ⁶, A. Yadav ⁴², A.K. Yadav ¹³⁴, Y. Yamaguchi ⁹¹, S. Yang ²⁰, S. Yano ⁹¹, E.R. Yeats ¹⁸, Z. Yin ⁶, I.-K. Yoo ¹⁶, J.H. Yoon ⁵⁸, H. Yu ¹², S. Yuan ²⁰, A. Yuncu ⁹³, V. Zaccolo ²³, C. Zampolli ³², F. Zanone ⁹³, N. Zardoshti ³², A. Zarochentsev ¹⁴⁰, P. Závada ⁶², N. Zaviyalov ¹⁴⁰, M. Zhalov ¹⁴⁰, B. Zhang ^{93,6}, C. Zhang ¹²⁹, L. Zhang ³⁹, M. Zhang ^{126,6}, M. Zhang ⁶, S. Zhang ³⁹, X. Zhang ⁶, Y. Zhang ¹¹⁹, Z. Zhang ⁶, M. Zhao ¹⁰, V. Zhrebchevskii ¹⁴⁰, Y. Zhi ¹⁰, D. Zhou ⁶, Y. Zhou ⁸², J. Zhu ^{54,6}, S. Zhu ¹¹⁹, Y. Zhu ⁶, S.C. Zugravel ⁵⁶, N. Zurlo ^{133,55}

Affiliation Notes

^I Deceased

^{II} Also at: Max-Planck-Institut für Physik, Munich, Germany

^{III} Also at: Italian National Agency for New Technologies, Energy and Sustainable Economic Development (ENEA), Bologna, Italy

^{IV} Also at: Dipartimento DET del Politecnico di Torino, Turin, Italy

^V Also at: Department of Applied Physics, Aligarh Muslim University, Aligarh, India

^{VI} Also at: Institute of Theoretical Physics, University of Wrocław, Poland

^{VII} Also at: Facultad de Ciencias, Universidad Nacional Autónoma de México, Mexico City, Mexico

Collaboration Institutes

¹ A.I. Alikhanyan National Science Laboratory (Yerevan Physics Institute) Foundation, Yerevan, Armenia

² AGH University of Krakow, Cracow, Poland

³ Bogolyubov Institute for Theoretical Physics, National Academy of Sciences of Ukraine, Kiev, Ukraine

⁴ Bose Institute, Department of Physics and Centre for Astroparticle Physics and Space Science (CAPSS), Kolkata, India

⁵ California Polytechnic State University, San Luis Obispo, California, United States

⁶ Central China Normal University, Wuhan, China

⁷ Centro de Aplicaciones Tecnológicas y Desarrollo Nuclear (CEADEN), Havana, Cuba

⁸ Centro de Investigación y de Estudios Avanzados (CINVESTAV), Mexico City and Mérida, Mexico

⁹ Chicago State University, Chicago, Illinois, United States

¹⁰ China Institute of Atomic Energy, Beijing, China

¹¹ China University of Geosciences, Wuhan, China

¹² Chungbuk National University, Cheongju, Republic of Korea

¹³ Comenius University Bratislava, Faculty of Mathematics, Physics and Informatics, Bratislava, Slovak Republic

¹⁴ Creighton University, Omaha, Nebraska, United States

¹⁵ Department of Physics, Aligarh Muslim University, Aligarh, India

¹⁶ Department of Physics, Pusan National University, Pusan, Republic of Korea

¹⁷ Department of Physics, Sejong University, Seoul, Republic of Korea

¹⁸ Department of Physics, University of California, Berkeley, California, United States

¹⁹ Department of Physics, University of Oslo, Oslo, Norway

²⁰ Department of Physics and Technology, University of Bergen, Bergen, Norway

²¹ Dipartimento di Fisica, Università di Pavia, Pavia, Italy

²² Dipartimento di Fisica dell'Università and Sezione INFN, Cagliari, Italy

²³ Dipartimento di Fisica dell'Università and Sezione INFN, Trieste, Italy

²⁴ Dipartimento di Fisica dell'Università and Sezione INFN, Turin, Italy

²⁵ Dipartimento di Fisica e Astronomia dell'Università and Sezione INFN, Bologna, Italy

²⁶ Dipartimento di Fisica e Astronomia dell'Università and Sezione INFN, Catania, Italy

²⁷ Dipartimento di Fisica e Astronomia dell'Università and Sezione INFN, Padova, Italy

²⁸ Dipartimento di Fisica 'E.R. Caianiello' dell'Università and Gruppo Collegato INFN, Salerno, Italy

²⁹ Dipartimento DISAT del Politecnico and Sezione INFN, Turin, Italy

³⁰ Dipartimento di Scienze MIFT, Università di Messina, Messina, Italy

³¹ Dipartimento Interateneo di Fisica 'M. Merlin' and Sezione INFN, Bari, Italy

³² European Organization for Nuclear Research (CERN), Geneva, Switzerland

³³ Faculty of Electrical Engineering, Mechanical Engineering and Naval Architecture, University of Split, Split, Croatia

- ³⁴ Faculty of Nuclear Sciences and Physical Engineering, Czech Technical University in Prague, Prague, Czech Republic
- ³⁵ Faculty of Physics, Sofia University, Sofia, Bulgaria
- ³⁶ Faculty of Science, P.J. Šafárik University, Košice, Slovak Republic
- ³⁷ Faculty of Technology, Environmental and Social Sciences, Bergen, Norway
- ³⁸ Frankfurt Institute for Advanced Studies, Johann Wolfgang Goethe-Universität Frankfurt, Frankfurt, Germany
- ³⁹ Fudan University, Shanghai, China
- ⁴⁰ Gangneung-Wonju National University, Gangneung, Republic of Korea
- ⁴¹ Gauhati University, Department of Physics, Guwahati, India
- ⁴² Helmholtz-Institut für Strahlen- und Kernphysik, Rheinische Friedrich-Wilhelms-Universität Bonn, Bonn, Germany
- ⁴³ Helsinki Institute of Physics (HIP), Helsinki, Finland
- ⁴⁴ High Energy Physics Group, Universidad Autónoma de Puebla, Puebla, Mexico
- ⁴⁵ Horia Hulubei National Institute of Physics and Nuclear Engineering, Bucharest, Romania
- ⁴⁶ HUN-REN Wigner Research Centre for Physics, Budapest, Hungary
- ⁴⁷ Indian Institute of Technology Bombay (IIT), Mumbai, India
- ⁴⁸ Indian Institute of Technology Indore, Indore, India
- ⁴⁹ INFN, Laboratori Nazionali di Frascati, Frascati, Italy
- ⁵⁰ INFN, Sezione di Bari, Bari, Italy
- ⁵¹ INFN, Sezione di Bologna, Bologna, Italy
- ⁵² INFN, Sezione di Cagliari, Cagliari, Italy
- ⁵³ INFN, Sezione di Catania, Catania, Italy
- ⁵⁴ INFN, Sezione di Padova, Padova, Italy
- ⁵⁵ INFN, Sezione di Pavia, Pavia, Italy
- ⁵⁶ INFN, Sezione di Torino, Turin, Italy
- ⁵⁷ INFN, Sezione di Trieste, Trieste, Italy
- ⁵⁸ Inha University, Incheon, Republic of Korea
- ⁵⁹ Institute for Gravitational and Subatomic Physics (GRASP), Utrecht University/Nikhef, Utrecht, Netherlands
- ⁶⁰ Institute of Experimental Physics, Slovak Academy of Sciences, Košice, Slovak Republic
- ⁶¹ Institute of Physics, Homi Bhabha National Institute, Bhubaneswar, India
- ⁶² Institute of Physics of the Czech Academy of Sciences, Prague, Czech Republic
- ⁶³ Institute of Space Science (ISS), Bucharest, Romania
- ⁶⁴ Institut für Kernphysik, Johann Wolfgang Goethe-Universität Frankfurt, Frankfurt, Germany
- ⁶⁵ Instituto de Ciencias Nucleares, Universidad Nacional Autónoma de México, Mexico City, Mexico
- ⁶⁶ Instituto de Física, Universidade Federal do Rio Grande do Sul (UFRGS), Porto Alegre, Brazil
- ⁶⁷ Instituto de Física, Universidad Nacional Autónoma de México, Mexico City, Mexico
- ⁶⁸ iThemba LABS, National Research Foundation, Somerset West, South Africa
- ⁶⁹ Jeonbuk National University, Jeonju, Republic of Korea
- ⁷⁰ Johann-Wolfgang-Goethe Universität Frankfurt Institut für Informatik, Fachbereich Informatik und Mathematik, Frankfurt, Germany
- ⁷¹ Korea Institute of Science and Technology Information, Daejeon, Republic of Korea
- ⁷² Laboratoire de Physique Subatomique et de Cosmologie, Université Grenoble-Alpes, CNRS-IN2P3, Grenoble, France
- ⁷³ Lawrence Berkeley National Laboratory, Berkeley, California, United States
- ⁷⁴ Lund University Department of Physics, Division of Particle Physics, Lund, Sweden
- ⁷⁵ Nagasaki Institute of Applied Science, Nagasaki, Japan
- ⁷⁶ Nara Women's University (NWU), Nara, Japan
- ⁷⁷ National and Kapodistrian University of Athens, School of Science, Department of Physics , Athens, Greece
- ⁷⁸ National Centre for Nuclear Research, Warsaw, Poland
- ⁷⁹ National Institute of Science Education and Research, Homi Bhabha National Institute, Jatni, India
- ⁸⁰ National Nuclear Research Center, Baku, Azerbaijan
- ⁸¹ National Research and Innovation Agency - BRIN, Jakarta, Indonesia
- ⁸² Niels Bohr Institute, University of Copenhagen, Copenhagen, Denmark
- ⁸³ Nikhef, National institute for subatomic physics, Amsterdam, Netherlands
- ⁸⁴ Nuclear Physics Group, STFC Daresbury Laboratory, Daresbury, United Kingdom
- ⁸⁵ Nuclear Physics Institute of the Czech Academy of Sciences, Husinec-Řež, Czech Republic

- ⁸⁶ Oak Ridge National Laboratory, Oak Ridge, Tennessee, United States
⁸⁷ Ohio State University, Columbus, Ohio, United States
⁸⁸ Physics department, Faculty of science, University of Zagreb, Zagreb, Croatia
⁸⁹ Physics Department, Panjab University, Chandigarh, India
⁹⁰ Physics Department, University of Jammu, Jammu, India
⁹¹ Physics Program and International Institute for Sustainability with Knotted Chiral Meta Matter (WPI-SKCM²), Hiroshima University, Hiroshima, Japan
⁹² Physikalischs Institut, Eberhard-Karls-Universität Tübingen, Tübingen, Germany
⁹³ Physikalischs Institut, Ruprecht-Karls-Universität Heidelberg, Heidelberg, Germany
⁹⁴ Physik Department, Technische Universität München, Munich, Germany
⁹⁵ Politecnico di Bari and Sezione INFN, Bari, Italy
⁹⁶ Research Division and ExtreMe Matter Institute EMMI, GSI Helmholtzzentrum für Schwerionenforschung GmbH, Darmstadt, Germany
⁹⁷ Saga University, Saga, Japan
⁹⁸ Saha Institute of Nuclear Physics, Homi Bhabha National Institute, Kolkata, India
⁹⁹ School of Physics and Astronomy, University of Birmingham, Birmingham, United Kingdom
¹⁰⁰ Sección Física, Departamento de Ciencias, Pontificia Universidad Católica del Perú, Lima, Peru
¹⁰¹ Stefan Meyer Institut für Subatomare Physik (SMI), Vienna, Austria
¹⁰² SUBATECH, IMT Atlantique, Nantes Université, CNRS-IN2P3, Nantes, France
¹⁰³ Sungkyunkwan University, Suwon City, Republic of Korea
¹⁰⁴ Suranaree University of Technology, Nakhon Ratchasima, Thailand
¹⁰⁵ Technical University of Košice, Košice, Slovak Republic
¹⁰⁶ The Henryk Niewodniczanski Institute of Nuclear Physics, Polish Academy of Sciences, Cracow, Poland
¹⁰⁷ The University of Texas at Austin, Austin, Texas, United States
¹⁰⁸ Universidad Autónoma de Sinaloa, Culiacán, Mexico
¹⁰⁹ Universidade de São Paulo (USP), São Paulo, Brazil
¹¹⁰ Universidade Estadual de Campinas (UNICAMP), Campinas, Brazil
¹¹¹ Universidade Federal do ABC, Santo Andre, Brazil
¹¹² Universitatea Nationala de Stiinta si Tehnologie Politehnica Bucuresti, Bucharest, Romania
¹¹³ University of Cape Town, Cape Town, South Africa
¹¹⁴ University of Derby, Derby, United Kingdom
¹¹⁵ University of Houston, Houston, Texas, United States
¹¹⁶ University of Jyväskylä, Jyväskylä, Finland
¹¹⁷ University of Kansas, Lawrence, Kansas, United States
¹¹⁸ University of Liverpool, Liverpool, United Kingdom
¹¹⁹ University of Science and Technology of China, Hefei, China
¹²⁰ University of South-Eastern Norway, Kongsberg, Norway
¹²¹ University of Tennessee, Knoxville, Tennessee, United States
¹²² University of the Witwatersrand, Johannesburg, South Africa
¹²³ University of Tokyo, Tokyo, Japan
¹²⁴ University of Tsukuba, Tsukuba, Japan
¹²⁵ Universität Münster, Institut für Kernphysik, Münster, Germany
¹²⁶ Université Clermont Auvergne, CNRS/IN2P3, LPC, Clermont-Ferrand, France
¹²⁷ Université de Lyon, CNRS/IN2P3, Institut de Physique des 2 Infinis de Lyon, Lyon, France
¹²⁸ Université de Strasbourg, CNRS, IPHC UMR 7178, F-67000 Strasbourg, France, Strasbourg, France
¹²⁹ Université Paris-Saclay, Centre d'Etudes de Saclay (CEA), IRFU, Département de Physique Nucléaire (DPhN), Saclay, France
¹³⁰ Université Paris-Saclay, CNRS/IN2P3, IJCLab, Orsay, France
¹³¹ Università degli Studi di Foggia, Foggia, Italy
¹³² Università del Piemonte Orientale, Vercelli, Italy
¹³³ Università di Brescia, Brescia, Italy
¹³⁴ Variable Energy Cyclotron Centre, Homi Bhabha National Institute, Kolkata, India
¹³⁵ Warsaw University of Technology, Warsaw, Poland
¹³⁶ Wayne State University, Detroit, Michigan, United States
¹³⁷ Yale University, New Haven, Connecticut, United States
¹³⁸ Yildiz Technical University, Istanbul, Turkey

¹³⁹ Yonsei University, Seoul, Republic of Korea

¹⁴⁰ Affiliated with an institute covered by a cooperation agreement with CERN

¹⁴¹ Affiliated with an international laboratory covered by a cooperation agreement with CERN.